JCB Journal of Cell Biology

ARTICLE

SARM1 acts downstream of neuroinflammatory and necroptotic signaling to induce axon degeneration

Kwang Woo Ko[1], Jeffrey Milbrandt[2,3], and Aaron DiAntonio[1,3]

Neuroinflammation and necroptosis are major contributors to neurodegenerative disease, and axon dysfunction and degeneration is often an initiating event. SARM1 is the central executioner of pathological axon degeneration. Here, we demonstrate functional and mechanistic links among these three pro-degenerative processes. In a neuroinflammatory model of glaucoma, TNF-α induces SARM1-dependent axon degeneration, oligodendrocyte loss, and subsequent retinal ganglion cell death. TNF-α also triggers SARM1-dependent axon degeneration in sensory neurons via a noncanonical necroptotic signaling mechanism. MLKL is the final executioner of canonical necroptosis; however, in axonal necroptosis, MLKL does not directly trigger degeneration. Instead, MLKL induces loss of the axon survival factors NMNAT2 and STMN2 to activate SARM1 NADase activity, which leads to calcium influx and axon degeneration. Hence, these findings define a specialized form of axonal necroptosis. The demonstration that neuroinflammatory signals and necroptosis can act locally in the axon to stimulate SARM1-dependent axon degeneration identifies a therapeutically targetable mechanism by which neuroinflammation can stimulate axon loss in neurodegenerative disease.

Introduction

While there are many different causes of neurodegenerative diseases, targeting common mechanisms promoting neuronal dysfunction and death would be a powerful approach for treating these devastating disorders. Early efforts to identify a common mechanism focused on neuronal apoptosis in hopes of blocking neuronal cell death. While tremendous strides were made in delineating the molecular mechanisms of apoptosis in neurons, targeting this pathway has not generated new treatments for neurodegeneration (Mattson, 2000; Maino et al., 2017). There are multiple reasons for this failure. First, we now know that there are many other cell death pathways that can kill neurons (Fuchs and Steller, 2015). Indeed, necroptosis is now appreciated to be a druggable pathway of programmed necrosis that is a very exciting target in many neurodegenerative diseases (Zhang et al., 2017; Yuan et al., 2019). Second, neurodegenerative diseases activate not only cell death pathways but also axonal death programs (Simon and Watkins, 2018). As synapse and axon loss is an early event in many neurodegenerative disorders (Coleman and Höke, 2020), mechanisms to maintain neuronal connectivity may need to be integrated with approaches for blocking neuronal cell death in order to maintain a functional nervous system. Finally, neurons are not the only cells affected in neurodegenerative diseases. In fact, neuroinflammation and microglial function is a central driver of many neurodegenerative diseases (Hickman et al., 2018; Perry and Holmes, 2014). Using both an in vivo glaucoma model and an in vitro neuronal culture model, we now explore functional and molecular links among neuroinflammatory signaling, necroptosis, and axonal degeneration.

Glaucoma is a neurodegenerative disease of retinal ganglion cells (RGCs) and a major preventable cause of blindness (Weinreb et al., 2014). While increases in intraocular pressure (IOP) are the proximate cause of most cases of glaucoma, neuroinflammation is a major contributor to the pathogenesis of glaucoma. Indeed, glaucoma can develop in the absence of IOP, and neurodegeneration can proceed even after successful restoration of normal pressures (Beidoe and Mousa, 2012). In both patients and rodent models, TNF-α is up-regulated in glaucomatous eyes (Yan et al., 2000; Sawada et al., 2010; Tezel et al., 2001). In experimental models, TNF-α is sufficient to activate microglia, stimulating a positive feedback loop that is capable of inducing RGC axon loss and eventual cell death (Nakazawa et al., 2006; Roh et al., 2012). Here, we used this neuroinflammatory model of glaucoma to test the hypothesis that SARM1 (sterile alpha and TIR motif 1), the central executioner of pathological axon degeneration, contributes to the pathogenesis of glaucoma.

[1]Department of Developmental Biology, Washington University School of Medicine, St. Louis, MO; [2]Department of Genetics, Washington University School of Medicine, St. Louis, MO; [3]Needleman Center for Neurometabolism and Axonal Therapeutics, Washington University School of Medicine, St. Louis, MO.

Correspondence to Aaron DiAntonio: diantonio@wustl.edu; Jeffrey Milbrandt: jmilbrandt@wustl.edu.

SARM1 is an inducible NAD^+ cleavage enzyme whose activation triggers metabolic catastrophe and axon degeneration in both classic injury-induced Wallerian degeneration and the dying back axon loss of peripheral neuropathy (Gerdts et al., 2016; Geisler et al., 2016; Essuman et al., 2017). Following optic nerve crush, SARM1 is required for distal RGC axon degeneration, but is not necessary for injury-dependent apoptosis and RGC death (Fernandes et al., 2018). While it is clear that SARM1 functions in RGCs to promote Wallerian degeneration, whether it acts in more disease-relevant models of RGC death is unknown. Overexpression of the fusion protein Wld^s, which includes the NAD^+ biosynthetic enzyme NMNAT1 (nicotinamide nucleotide adenylyltransferase 1) and so can inhibit SARM1 (Sasaki et al., 2016), has given conflicting results in glaucoma models. Wld^s can protect axons but not cell bodies in a rat glaucoma model (Beirowski et al., 2008), while the coadministration of the NAD^+ precursor nicotinamide in conjunction with Wld^s (Williams et al., 2017a) or the overexpression of cytosolically targeted NMNAT1 enzyme (Zhu et al., 2013) can protect axons and cell bodies. Whether NMNAT1/Wld^s is primarily augmenting NAD^+ biosynthesis or inhibiting SARM1 in these paradigms is unknown. Hence, it is important to test the requirement for SARM1 directly in a glaucoma model, in particular because SARM1 is an enzyme and so a druggable target (DiAntonio, 2019). Finally, mechanisms of SARM1 activation are well understood in Wallerian degeneration, where axotomy blocks delivery of labile axon survival factors that inhibit SARM1 (Figley and DiAntonio, 2020). However, whether and how other disease processes activate SARM1 are not known.

Here, we test the role of SARM1 in a neuroinflammatory model of glaucoma, demonstrating that SARM1 is required for RGC axon loss, RGC death, and oligodendrocyte death following intravitreal TNF-α application. We show that oligodendrocyte death is secondary to axon loss in this glaucoma model using a therapeutically translatable adeno-associated virus (AAV) gene therapy approach to express a SARM1 dominant-negative transgene (Geisler et al., 2019b). We explore the mechanisms linking TNF-α signaling to SARM1 in neuronal culture, demonstrating that in a TNF-α–dependent neuronal necroptosis model, SARM1 induces axon degeneration. Our findings demonstrate that in contrast to canonical necroptotic cell death in which MLKL (mixed lineage kinase domain-like pseudokinase) is the final executioner, there exists a specialized "axonal necroptosis" process in which MLKL works through the SARM1 axon degeneration pathway to drive axon demise. Activated MLKL induces loss of the axon survival factors NMNAT2 and SCG10/STMN2, known inhibitors of SARM1 activation that are also lost following axotomy, chemotherapy-induced neurotoxicity, and mitochondrial dysfunction (Geisler et al., 2019a; Loreto et al., 2020; Summers et al., 2020; Gilley et al., 2015). Hence, disparate upstream pro-degenerative signals converge on these axon survival factors to activate SARM1. These studies identify molecular mechanisms linking neuroinflammation, necroptosis, and SARM1 activation, and suggest that local inflammatory signaling in the axon may drive SARM1-dependent axon loss. This unification of three major drivers of neurodegeneration may have broad implications for treatment of neurological diseases.

Results

TNF-α induces SARM1-dependent axon loss and RGC death in a neuroinflammatory model of glaucoma

Glaucoma is a neurodegenerative disease in which increased IOP leads to neuroinflammation, triggering loss of optic nerve axons and subsequent death of RGCs (Tezel and Wax, 2004; Bosco et al., 2011; Williams et al., 2017b, 2017c). SARM1 is the central executioner of axon degeneration in other pathological conditions (Henninger et al., 2016; Geisler et al., 2016), and we therefore investigated whether SARM1 promotes the loss of RGC axons in response to TNF-α injection into the vitreous cavity (Fig. 1 A), an established neuroinflammatory model of glaucoma.

We injected TNF-α or PBS into the vitreous cavity of 5-wk-old WT and SARM1 knockout (KO) mice. We assessed axon number in the optic nerve via EM and RGC number via Brn3a staining of cell bodies in retinal whole mounts at 2 wk and 2 mo after treatment. In this model, axon loss occurs by 2 wk, while RGC loss is complete by 2 mo (Kitaoka et al., 2006, 2009, 2013; Nakazawa et al., 2006; Roh et al., 2012). In agreement with prior findings, optic nerves from TNF-α–treated WT eyes demonstrated an ∼37% reduction in axon number, a degree of degeneration that would likely lead to abnormalities in visual field testing in human patients (Kerrigan-Baumrind et al., 2000). In WT axons, there is also a concomitant ∼26% increase in axon size after 2 wk (Fig. 1, C and D). Analysis of the distribution of axon sizes at 2 wk does not indicate the loss of a distinct cohort of axons, as the distribution of axon sizes is similar between PBS and TNF-α–treated WT axons (Fig. 2 E). In contrast, TNF-α treatment in SARM1 KO mice did not lead to significant differences in optic nerve axon number or axon size. There is no significant further loss of axons 2 mo following TNF-α injection in WT mice; however, there is a continued increase in axon size, driven largely by a population of large axons (>1.6 µm) that are not apparent in PBS-treated or -untreated optic nerve (Fig. 1, B–E). In contrast, SARM1 KO mice remain resistant to the effects of intravitreal TNF-α injection, showing no significant loss of total axon number or increase in axon size at 2 mo following TNF-α treatment (Fig. 1, B–E). Hence, there is not merely a delay in axon degeneration in SARM1 KO mice; instead, SARM1 is required for axon loss in this TNF-α–triggered glaucoma model.

Having assessed axon number, we next quantified RGC survival following intravitreal TNF-α injection. We stained retinas with Brn3a to identify RGCs. While no RGC loss was observed at 2 wk (Kitaoka et al., 2006, 2009), there was significant loss of RGCs in WT retinas 2 mo after TNF-α treatment (Fig. 1, F and G). SARM1 KO mice were fully resistant to TNF-α–induced RGC death, showing no significant decrease in RGC cell number at 2 mo (Fig. 1, F and G). Hence, loss of SARM1 protects both RGC axons and cell bodies in this model of TNF-α–triggered glaucoma. The temporal pattern of axon and cell body loss is consistent with the idea that RGC death is a consequence of axon degeneration.

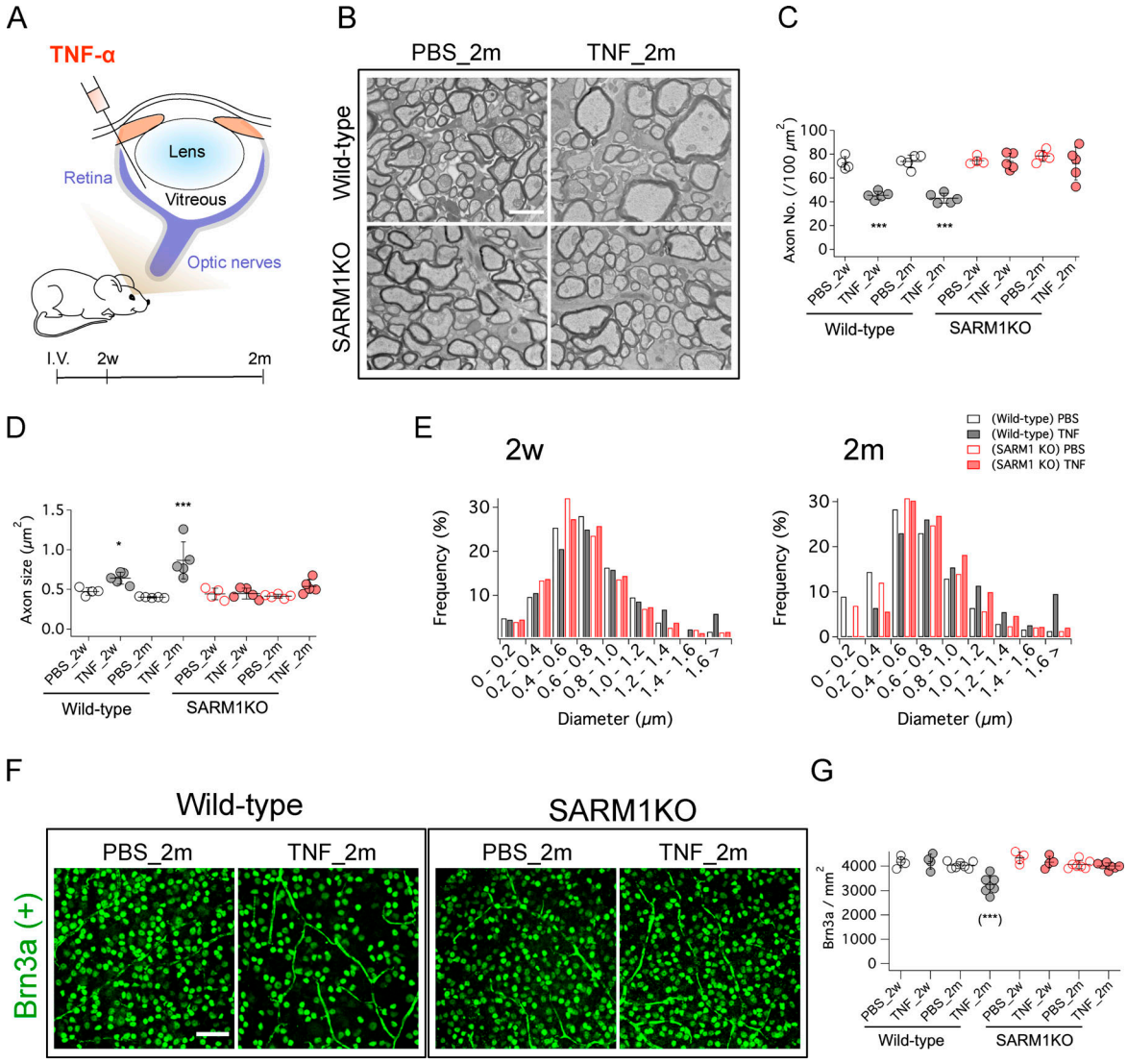

Figure 1. **TNF-α induces SARM1-dependent axon loss and RGC death in a neuroinflammatory model of glaucoma. (A)** Schematic diagram of TNF-α intravitreal (I.V.) injection. Axons and cell bodies are quantified at 2 wk (2w) or 2 mo (2m) following TNF-α or PBS injection. **(B)** EM of WT and SARM1 KO optic nerves at 2 mo after PBS or TNF-α injection. Scale bar, 2 µm. **(C and D)** Quantification of axon number (C) and axon size (D) in the optic nerve of WT or SARM1 KO mice at 2 wk (2w) or 2 mo (2m) after intravitreal injection of PBS or TNF-α. Data represent the mean ± SEM; *n* = 4 or 5 for each condition; (C) axon number: one-way ANOVA with post hoc Tukey test, $F(7,30) = 21.1$, $P < 0.0001$; (D) axon size: One-way ANOVA with post hoc Tukey test, $F(7,34) = 15.27$, $P < 0.0001$; *, $P < 0.05$; **, $P < 0.01$; and ***, $P < 0.001$. **(E)** Histograms of the range of axon diameter at 2 wk (2w, left) and 2 mo (2m, right). Data are the same as used in C and D. **(F)** Representative Brn3a immunostaining of WT and SARM1 KO retinas at 2 mo after TNF-α injection. Scale bar, 50 µm. **(G)** Quantification of the number of Brn3a-positive RGCs in WT or SARM1 KO retina at 2 wk (2w) or 2 mo (2m) after PBS or TNF-α intravitreal injection. Data represent the mean ± SEM; *n* = 4–7 for each condition; One-way ANOVA with post hoc Tukey test, $F(7,36) = 13.2$, $P < 0.0001$; *, $P < 0.05$; **, $P < 0.01$; and ***, $P < 0.001$.

SARM1 is required for TNF-α–dependent oligodendrocyte death but not microglial activation

Having demonstrated that loss of SARM1 protects RGC axons and cell bodies from TNF-α–induced degeneration, we next assessed whether SARM1 influenced other TNF-α–dependent events. Intravitreal TNF-α injection activates microglia that then amplify the inflammatory response (Nakazawa et al., 2006; Roh et al., 2012; Son et al., 2010). To quantify microglial activation, we measured the size of microglial soma, as soma size increases upon microglial activation while processes become less complex (Davis et al., 2017). Intravitreal injection can temporarily activate microglia (Seitz and Tamm, 2014), so we first performed control intravitreal PBS injections. In WT mice, microglial soma size increased within 1 d and returned to a normal soma size with more complex processes by 3 d. In age-matched SARM1 KO mice, microglial soma size was also normal 3 d following intravitreal PBS injection (Fig. 2, A and B). In contrast, intravitreal TNF-α injection led to microglial activation in both WT and SARM1 KO retina that persisted for at least 1 wk (Fig. 2, A and B). Therefore, intravitreal TNF-α stimulates a sustained neuroinflammatory response in the retina that is not SARM1-dependent. Hence, SARM1 is likely acting downstream of this neuroinflammatory response to promote axon loss and RGC death.

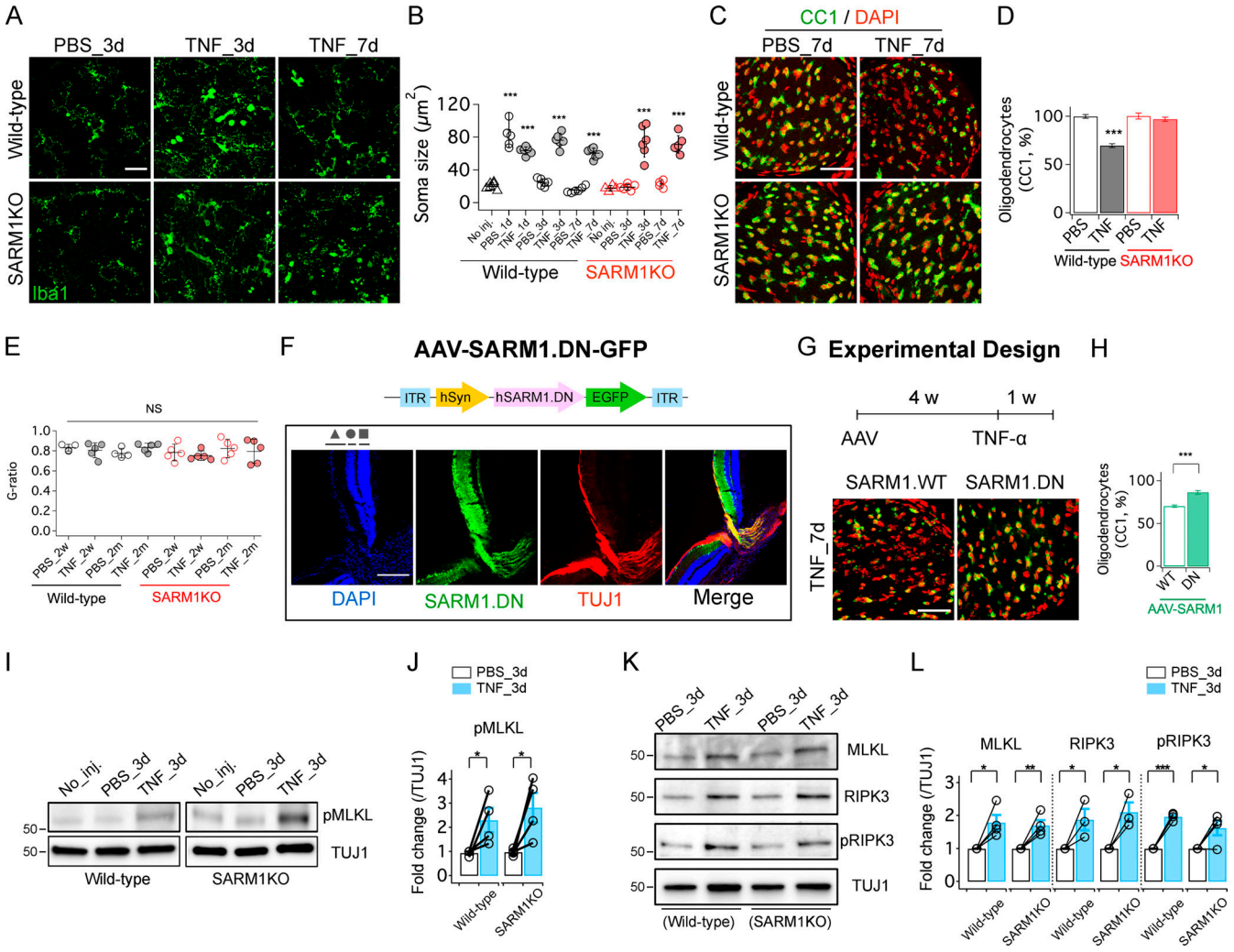

Figure 2. **SARM1 mediates RGC and oligodendrocyte death in a neuroinflammatory model of glaucoma. (A)** Representative Iba1 immunostaining of WT and SARM1 KO retinas at 3 or 7 d after TNF-α or PBS intravitreal injection. Scale bar, 50 µm. **(B)** Quantification of microglial soma size at various times after intravitreal injection of PBS or TNF-α of WT or SARM1 KO animals (No inj.: intact eye without injection). Data represent the mean ± SEM; n = 4–6 for each condition; one-way ANOVA with post hoc Tukey test, F(11,56) = 44.8, P < 0.0001; *, P < 0.05; **, P < 0.01; and ***, P < 0.001. **(C)** Representative CC1 and DAPI immunostaining of WT and SARM1 KO optic nerves (cross-section) 7 d after TNF-α or PBS injection. Scale bar, 50 µm. **(D)** Quantification of mature oligodendrocytes in WT and SARM1 KO optic nerves at 7 d after PBS or TNF-α treatment. Data are displayed as a percentage of oligodendrocytes present in WT eyes injected with PBS. Data are represented as mean ± SEM; n = 4; One-way ANOVA with post hoc Tukey test, F(3,12) = 41.78, P < 0.0001; *, P < 0.05; **, P < 0.01; and ***, P < 0.001. **(E)** Quantification of G-ratio. The EM images used in Fig. 1, C and D, were analyzed. Data represent the mean ± SEM; n = 4–5 for each condition; one-way ANOVA with post hoc Tukey test, F(7,30) = 0.7174, P = 0.6580; NS, not significant; *, P < 0.05; **, P < 0.01; and ***, P < 0.001. **(F)** Top: Schematic diagram of AAV vector expressing human SARM1.DN (hSARM1.DN) under control of neuron-specific hSyn. Bottom: Representative retinal cross-section. SARM1.DN protein (green) is present in the RGC layer (triangle) and RGC axons that colabel with TUJ1 (red). Inner nuclear layer (circle), outer nuclear layer (square), cell bodies (DAPI, blue). Scale bar, 0.2 mm. **(G)** Top: Virus expressing WT SARM1 (AAV.SARM1.WT) or AAV.SARM1.DN is delivered via intravitreal injection into WT mice. 4 wk later, TNF-α is injected intravitreally, and oligodendrocytes are quantified 7 d later. Bottom: Representative CC1 and DAPI immunostaining of SARM1.WT or SARM1.DN-expressing optic nerve 7 d after TNF-α injection. Scale bar, 50 µm. **(H)** Quantification from G of the number of mature oligodendrocytes following TNF-α injection (displayed as a percentage relative to the number observed in WT nerve following PBS intravitreal injection). Data are represented as mean ± SEM, n = 4; two-tailed unpaired t test, SARM1.WT versus SARM1.DN, P = 0.0007; *, P < 0.05; **, P < 0.01; and ***, P < 0.001. **(I)** Immunoblot for pMLKL from optic nerve extracts derived from WT or SARM1 KO animals 3 d after intravitreal injection of TNF-α or PBS or uninjected control (No_inj). TUJ1 was used as a loading control. **(J)** Quantification of pMLKL expression from immunoblots. TUJ1 signal was used for normalization. Data represent the mean ± SEM, n = 4; two-tailed unpaired t test, (WT) PBS_3d versus TNF_3d, P = 0.03; (SARM1KO) PBS_3d versus TNF_3d, P = 0.02; *, P < 0.05; **, P < 0.01; and ***, P < 0.001. **(K)** Immunoblot for MLKL, RIPK3, and phosphorylated RIPK3 (pRIPK3) from optic nerve extracts derived from WT or SARM1 KO animals 3 d after intravitreal injection of TNF-α or PBS. TUJ1 was used as a loading control. **(L)** Quantification of the intensity of MLKL (n = 4), RIPK3 (n = 3), and pRIP3 (n = 4) from immunoblots. TUJ1 signal was used for normalization. Data represent the mean ± SEM; two-tailed unpaired t test; (MLKL, WT) PBS_3d versus TNF_3d, P = 0.014; (MLKL, SARM1 KO) PBS_3d versus TNF_3d, P = 0.005; (RIPK3, WT) PBS_3d versus TNF_3d, P = 0.028; (RIPK3, SARM1 KO) PBS_3d versus TNF_3d, P = 0.018; (pRIPK3, WT) PBS_3d versus TNF_3d, P = 1.9E-06; (pRIPK3, SARM1 KO) PBS_3d versus TNF_3d, P = 0.03; *, P < 0.05; **, P < 0.01; and ***, P < 0.001.

While RGC death is central to the pathogenesis of glaucoma, oligodendrocytes in the optic nerve are also lost in models of glaucoma (Nakazawa et al., 2006; Son et al., 2010). Oligodendrocytes both insulate and provide metabolic support to RGC axons in the optic nerve, and so we investigated whether oligodendrocytes are also preserved in the absence of SARM1 in this glaucoma model. We stained for CC1, a marker of nonproliferative mature oligodendrocytes (Payne et al., 2013), in the optic nerves of TNF-α–treated WT and SARM1 KO mice. In WT mice, TNF-α treatment decreased the number of CC1-positive oligodendrocytes by ∼30% after 1 wk. Despite this loss in oligodendrocyte number, there is no change in the G-ratio of surviving axons (Fig. 2 E). Hence, oligodendrocyte loss likely occurs concomitantly with axon loss, rather than inducing aberrant myelination of surviving axons. In SARM1 KO animals, TNF-α treatment induced no significant loss of oligodendrocytes in the optic nerve (Fig. 2, C and D). Hence, SARM1 is required for oligodendrocyte death in response to neuroinflammatory signaling.

The preservation of oligodendrocytes in TNF-α–treated SARM1 KO mice could reflect a cell-autonomous action of SARM1 in oligodendrocytes to drive cell death, or alternatively a noncell autonomous role for axons in maintaining oligodendrocytes. To distinguish between these possibilities, we took advantage of a dominant-negative SARM1 (SARM1.DN) that potently blocks SARM1 function in vivo following viral delivery (Geisler et al., 2019b). SARM1-DN fused to EGFP or WT SARM1 fused to EGFP were cloned into an AAV vector and expressed under control of the neuron-specific human synapsin (hSyn) promoter. A combination of the 7m8 capsid (Dalkara et al., 2013; Büning and Srivastava, 2019) and hSyn promoter enabled robust retinal expression that is limited to neurons (Fig. 2 F). 4 wk after intravitreal injection of AAV2-hSyn-SARM1-DN-EGFP (AAV-SARM1.DN) or control virus (AAV-SARM1.WT), we observed robust EGFP labeling of RGCs and axons (Fig. 2 F; and Fig. S1, A and B). In contrast, we do not observe expression in oligodendrocytes in the optic nerve (Fig. S1, C and D), allowing us to test whether neuron-specific inhibition of SARM1 is sufficient to block TNF-α induced oligodendrocyte death. Expression of WT SARM1 (AAV-SARM1.WT) showed the expected loss of oligodendrocytes 1 wk after intravitreal injection of TNF-α. In contrast, oligodendrocyte loss was significantly attenuated by expression of the SARM1-DN in RGCs (Fig. 2, G and H). These findings indicate that loss of oligodendrocytes is secondary to SARM1-dependent function in RGCs, and suggests that maintenance of healthy axons is required for oligodendrocyte survival in response to neuroinflammatory signals.

Taken together, this series of experiments demonstrates that SARM1 does not block the ability of TNF-α to induce neuroinflammatory stimulation of microglia, but is required for subsequent oligodendrocyte death, axon loss, and RGC cell death. Hence, SARM1 is an essential downstream mediator of neuroinflammatory damage in this model of glaucoma, and so is a candidate therapeutic target for preventing neurodegeneration in glaucoma.

Having explored the cellular consequences of intravitreal TNF-α injection, we next investigated activation of pro-degenerative molecular pathways. TNF-α can trigger apoptosis or necroptosis in different contexts, including in promoting RGC death in models of glaucoma (Fuchs and Steller, 2015; Weinlich et al., 2017; Do et al., 2017; Almasieh et al., 2012). Hence, we used immunoblotting to assess molecular markers of apoptosis and necroptosis in the optic nerve following intravitreal TNF-α injection. We did not detect cleaved caspase 3 via immunoblotting of optic nerve from TNF-α–injected eyes of either WT or SARM1 KO mice (Fig. S2 A), consistent with our previous demonstration that SARM1 does not participate in apoptosis (Gerdts et al., 2013). We next investigated whether intravitreal TNF-α activates necroptosis, an inflammatory form of programmed cell death (Kearney and Martin, 2017; Silke et al., 2015; Heckmann et al., 2019). To assess activation of necroptotic signaling, we assayed levels and phosphorylation of RIPK3 and MLKL, two essential proteins for necroptosis (Ofengeim et al., 2015; Caccamo et al., 2017; Ito et al., 2016; Vitner et al., 2014). At 3 d following intravitreal injection of TNF-α or PBS into WT and SARM1 KO mice, we harvested optic nerves and performed immunoblot analysis. In response to TNF-α injection, there was a significant increase in the levels of phosphorylated MLKL, total MLKL, phosphorylated RIPK3, and total RIPK3 in optic nerves of both WT and SARM1 KO mice (Fig. 2, I–L). Similar induction of necroptotic signaling proteins is detected in other neurodegenerative diseases (Ofengeim et al., 2015; Caccamo et al., 2017; Vitner et al., 2014; Ito et al., 2016; Zhang et al., 2017). Hence, TNF-α activates necroptotic signaling in the optic nerve in a SARM1-independent manner, suggesting that SARM1 may function downstream of necroptosis to promote axon degeneration and cell death.

A TNF-α–dependent neuronal necroptosis model triggers SARM1-dependent axon degeneration in sensory neurons

To explore the relationships among TNF-α, necroptosis, and SARM1, we turned to cultured dorsal root ganglion (DRG) neurons, a pure neuronal population amenable to a mechanistic analysis of axon degeneration (Fig. 3 A). We first developed a TNF-α–dependent in vitro model of necroptosis in DRG neurons. As there is cross-talk between apoptosis and necroptosis (Heckmann et al., 2019), in cultured cells TNF-α can be biased to stimulate necroptosis by simultaneously inhibiting apoptosis with Z-VAD (carbobenzoxy-valyl-alanyl-aspartyl-[O-methyl]-fluoromethylketone) and blocking survival signaling with a SMAC (second mitochondria-derived activator of caspases) mimetic (Gong et al., 2017; Wang et al., 2012). Using this cocktail, we found that TNF-α treatment of DRG neurons induces the phosphorylation of MLKL. This increase in phosphorylated MLKL is blocked by necrostatin-1s, an inhibitor of RIPK1, a key component of the necrosome required for MLKL phosphorylation during necroptosis (Fig. 3 B). Next, we assessed whether TNF-α triggers axon degeneration in cultured DRG neurons. Axons were imaged over time using an Operetta high-content imaging system. Axon morphology was assessed via bright-field imaging, and axonal energetics were examined using tetramethylrhodamine methylester (TMRM), a fluorescent reporter of mitochondrial potential. TNF-α induced axonal swelling by 48 h and progressed to frank degeneration by 72 h, at which point

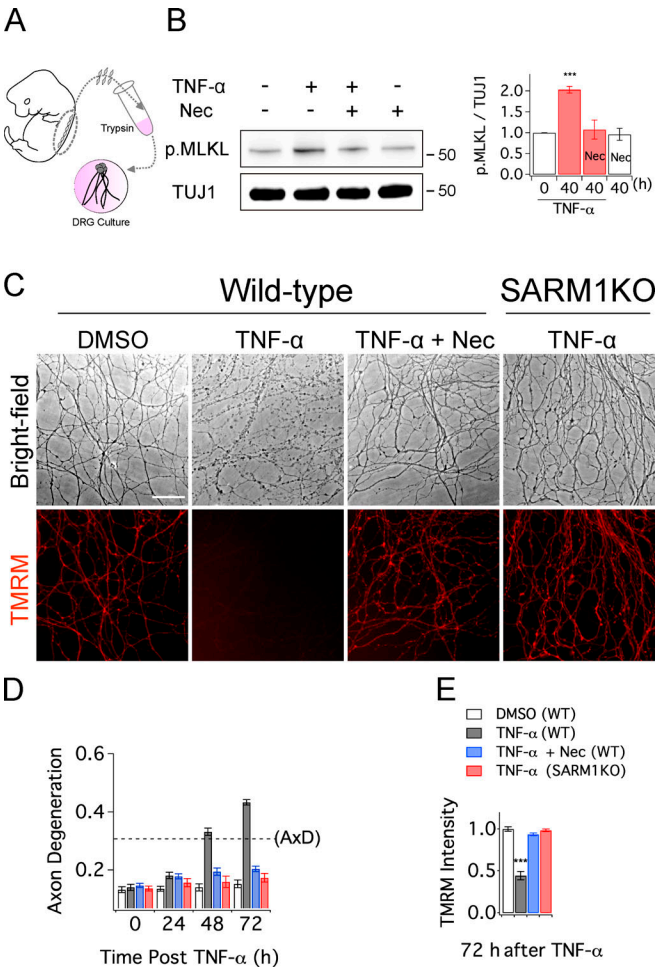

Figure 3. **TNF-α induces neuronal necroptosis and SARM1-dependent axon degeneration in sensory neurons. (A)** Schematic of embryonic day 13.5 DRG culture system. **(B)** Left: DRG neurons are treated with the indicated compounds and axon-only extracts are immunoblotted for pMLKL. TNF-α (100 ng/ml) is applied together with SMAC mimetic (LCL161, 10 µM) and pan caspase inhibitor Z.VAD (100 µM). Necrostatin-1s (Nec), 20 µM. Right: Quantification of pMLKL protein levels normalized to TUJ1 levels. Data are represented as mean ± SEM, $n = 3$; one-way ANOVA with post hoc Tukey test, $F(3,8) = 13.04$, $P = 0.0019$; *, $P < 0.05$; **, $P < 0.01$; and ***, $P < 0.001$. **(C)** Representative bright-field and TMRM images of cultured DRG axons from WT or SARM1 KO neurons treated with TNF-α (together with 10 µM LCL161, 100 µM Z.VAD) and necrostatin as indicated. Scale bar = 50 µm. **(D)** DRG neurons from WT or SARM1 KO mice were treated with TNF-α (together with 10 µM LCL161 and 100 µM Z.VAD) and necrostatin where indicated. Axon degeneration was quantified from bright-field images at the indicated time points after TNF-α application. Axons with a DI >0.3 are defined as degenerated (dashed line). Data represent the mean ± SEM, $n = 5$; two-way ANOVA with post hoc Bonferroni's multiple comparison test; time, $F(2.217, 35.48) = 256$, $P < 0.0001$; interaction, $F(16,48) = 13.41$, $P < 0.0001$; *, $P < 0.05$; **, $P < 0.01$; and ***, $P < 0.001$. **(E)** Quantification of TMRM intensity in axons after 72 h of TNF-α treatment (as described in D). TMRM (50 nM) was applied 30 min before image acquisition. Data represent the mean ± SEM, $n = 3$; one-way ANOVA with post hoc Tukey test, $F(3,8) = 71.72$, $P < 0.0001$; *, $P < 0.05$; **, $P < 0.01$; and ***, $P < 0.001$.

there was a dramatic loss in TMRM signal (Fig. 3 C). This TNF-α–induced axon degeneration is driven by necroptosis, as it is prevented in the presence of necrostatin-1s. Importantly, both the TNF-α–induced axonal degeneration and loss of mitochondrial potential are fully blocked in SARM1 KO neurons (Fig. 3, C–E). Hence, TNF-α and necroptosis require SARM1 to induce axon degeneration. While this cytokine-induced axon degeneration is slower than axotomy-induced axon degeneration, the common requirement for SARM1 demonstrates that neuroinflammatory and necroptotic signaling in the axon share molecular mechanisms with Wallerian degeneration.

Direct activation of necroptosis triggers SARM1-dependent axon degeneration

While TNF-α can activate a model of necroptosis in DRG neurons, in other cell types it can activate multiple death pathways (Weinlich et al., 2017; Kearney and Martin, 2017; Heckmann et al., 2019), making it more difficult to dissect the mechanistic relationship between necroptosis and SARM1-dependent degeneration. To test directly the hypothesis that SARM1 functions downstream of necroptosis, we used an engineered variant of MLKL that allows for temporal and spatial induction of necroptosis (Gong et al., 2017; Orozco et al., 2014; Fegan et al., 2010; Zhang et al., 2016). The N-terminal domain of MLKL (MLKL.ND) was fused to $Fkbp^{F36v}$ (Fig. 4 A, labeled with yellow), a protein whose dimerization is induced in the presence of the rapamycin analogue B/B homodimerizer (BB; star). Forced dimerization of MLKL.ND with BB in DRG neurons shows several features of necroptosis within 24 h (Fig. 4 B), including loss of cytosolic GFP consistent with membrane rupture, externalization of phosphatidylserine as shown by annexin V staining, and cell death as marked by nuclear accumulation of ethidium homodimer (EthD), which does not enter live cells (Fig. 4 B). Interestingly, a few neurons with annexin V membrane staining (arrowhead, BB_24hr panel) show intact GFP fluorescence in cytosol and no EthD fluorescence, suggesting that they are still alive. These findings are consistent with the loss of membrane asymmetry induced by ATP depletion or dysfunction of ATP-dependent enzymes preceding membrane rupture during necroptosis (Gong et al., 2017; Hankins et al., 2015). Taken together, these findings show dimerized MLKL.ND causes necroptosis in DRG neurons.

We next tested whether necroptosis induced by dimerization of MLKL.ND triggers axon degeneration and assessed the requirements for signaling proteins. We find that dimerization of MLKL.ND causes axon degeneration and loss of TMRM staining of WT axons within 24 h. Direct dimerization of MLKL.ND should bypass the requirement for upstream RIPK activity, and as predicted the RIPK1 inhibitor necrostatin-1s did not prevent axon degeneration following dimerization of MLKL.ND (Fig. S3, A and B). Dimerized MLKL.ND can interact with endogenous MLKL to mediate downstream necroptotic signaling (Tanzer et al., 2016). We knocked down MLKL with an shRNA targeting the C terminus of MLKL, so that it would not impact the levels of the dimerizable MLKL.ND construct, and validated the efficacy of the shRNA in both DRG neurons and in N2A cells that express high levels of MLKL (Fig. S4). Upon knockdown of endogenous MLKL, the dimerization of MLKL.ND does not trigger axon degeneration (Fig. S5 A). In addition, the dimerization of MLKL.ND increases the level of phosphorylated full-length MLKL, and this is not blocked by necrostatin (Fig. S5, B and C).

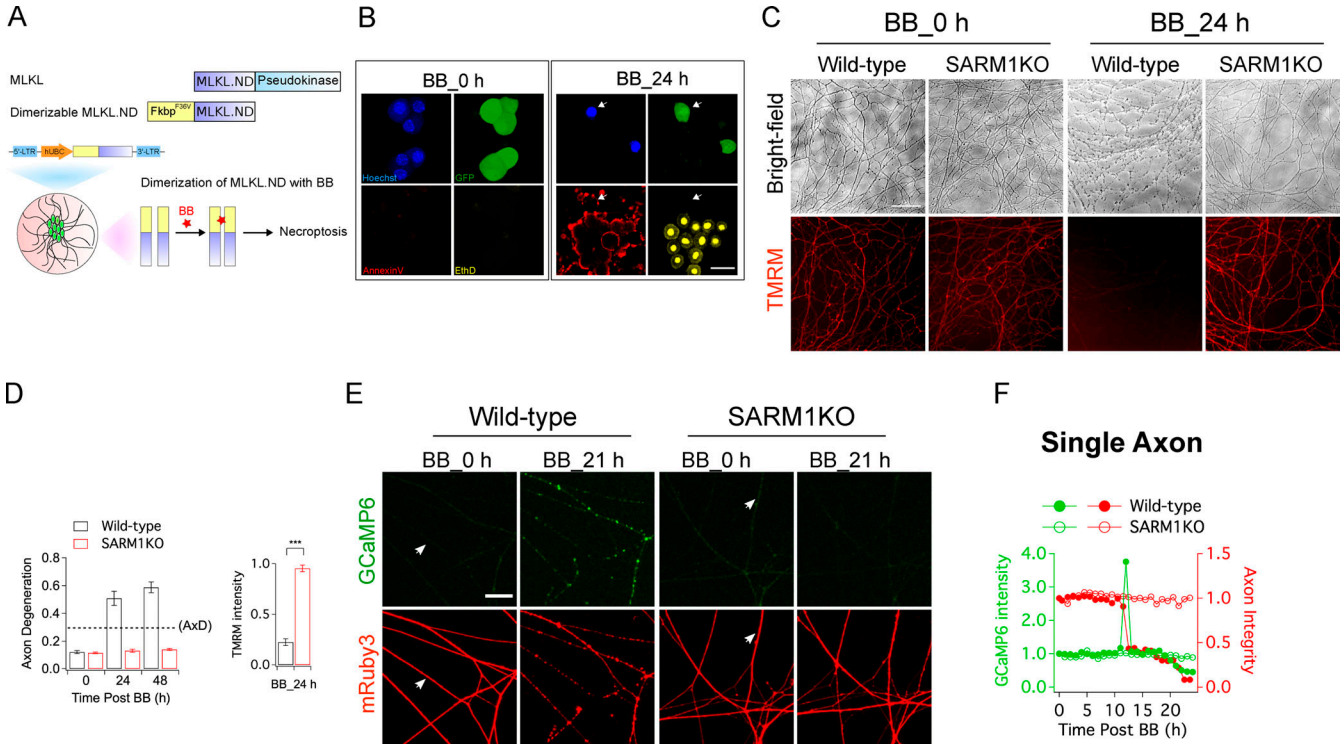

Figure 4. **Direct activation of necroptosis triggers SARM1 dependent axon degeneration. (A)** Top: Schematic of MLKL and dimerizable MLKL.ND construct (MLKL.ND = MLKL N-terminal domain) used in this study. MLKL.ND is fused to $Fkbp^{F36V}$. Bottom: Neurons are infected with lentivirus expressing MLKL.ND, and dimerization is induced with BB (100 nM) to promote necroptosis. **(B)** Representative images of cell bodies of cultured DRG neurons expressing MLKL.ND at baseline (left) and 24 h after BB (100 nM) application (right). After 24 h, most cells have died from necroptosis (lose both Hoechst staining and soluble GFP fluorescence: gain both annexin V and EthD staining). In two cells (arrow), annexin V is detected before EthD staining or loss of both Hoechst and cytosolic GFP, suggesting that annexin V staining is an early sign of impending cell death. Hoechst (blue), cytosolic GFP (green), annexin V (red), EthD (yellow); scale bar, 30 µm. **(C)** Representative bright-field and TMRM images of axons from WT and SARM1 KO DRG neurons expressing MLKL.ND at baseline (left) and 24 h after BB (100 nM) treatment (right). Scale bar, 50 µm. **(D)** Quantification of axon degeneration (left, n = 5) and TMRM intensity (right, n = 3) at the indicated time points after BB (100 nM) addition to WT or SARM1 KO neurons. Axons with a DI >0.3 are defined as degenerated (dashed line). Data represent the mean ± SEM. For axon degeneration, two-way ANOVA with post hoc Bonferroni's multiple comparison test; time, $F(2,16) = 106.5$, $P < 0.0001$; interaction, $F(8,16) = 4.635$, $P = 0.0044$. For TMRM, two-tailed unpaired t test, $P < 0.0001$; *, $P < 0.05$; **, $P < 0.01$; and ***, $P < 0.001$. **(E)** Representative fluorescent images of WT or SARM1 KO axons infected with lentivirus encoding the calcium reporter GCaMP6, the axon integrity reporter mRuby3, and MLKL.ND at baseline and 21 h after BB application. Scale bar, 30 µm. **(F)** Depiction of Ca^{2+} dynamics with GCaMP6 fluorescent intensity (green, left y axis), and axon integrity with mRuby3 fluorescent intensity (red, right y axis) from a representative single axon of each genotype from E (arrowhead).

Hence, in this system, dimerized MLKL.ND recruits endogenous MLKL to mediate downstream axon degeneration.

With this system in hand, we asked if axon degeneration induced by MLKL.ND dimerization requires SARM1. In contrast to WT neurons, axons from SARM1 KO neurons were fully protected from both axon degeneration and loss of mitochondrial potential for at least 48 h after MLKL.ND dimerization (Fig. 4, C and D). We also assessed calcium influx, a common feature of necroptosis and Wallerian degeneration. While the mechanism of calcium influx during necroptosis is not fully understood, there is a consensus that calcium influx is the consequence of membrane permeabilization induced by MLKL (Wang et al., 2014; Su et al., 2014; Cai et al., 2014; Xia et al., 2016). We used live-cell imaging to simultaneously monitor intracellular calcium using GCaMP6 (Chen et al., 2013) and axonal integrity with mRuby3, a photostable fluorescent cytosolic protein (Bajar et al., 2016). In WT axons, dimerization of MLKL.ND triggered calcium influx and axon degeneration that was completely prevented in axons from SARM1 KO neurons (Fig. 4, E and F; and Video 1). This is a surprising finding, since in other systems MLKL induces calcium influx via direct membrane permeabilization. In contrast, in axonal necroptosis, SARM1 becomes activated and triggers calcium influx and axon degeneration. Interestingly, this relationship is selective for the axon, as in the cell body the activation of necroptosis via dimerization of MLKL.ND triggered calcium influx followed by membrane rupture in both WT and SARM1 KO neurons (Video 1). Indeed, there is no significant difference in the extent of cell death induced by necroptosis in WT versus SARM1 KO neurons (Fig. S6). Taken together, these findings suggest the exciting hypothesis that canonical necroptotic signaling drives cell death in sensory neurons, but that a specialized form of axonal necroptosis uses a distinct SARM1-dependent mechanism to trigger calcium influx and axon degeneration.

As a first test of this hypothesis, we investigated whether other components of the SARM1 Wallerian degeneration pathway function downstream of necroptosis for axon degeneration. In classical Wallerian degeneration, overexpression of the axon

survival factor cytoNMNAT1 and inhibition of the neuronal stress kinases DLK (dual leucine zipper kinase) and LZK (leucine zipper-bearing kinase) potently inhibit axotomy-induced axon degeneration (Summers et al., 2018). Upon MLKL.ND dimerization-induced necroptosis, cytoNMNAT1 overexpression and treatment with the DLK/LZK inhibitor GNE-3511 both potently block axon degeneration (Fig. S7). These findings support the hypothesis that axonal necroptosis can stimulate the canonical Wallerian degeneration program to drive axon loss. DLK inhibition can block apoptotic neuronal cell death (Ghosh et al., 2011), but as with SARM1 KO, does not block necroptotic cell death induced by MLKL.ND dimerization (Fig. S7). These findings highlight that necroptosis-induced cell death and necroptosis-induced axon degeneration are mechanistically distinct.

Axonal necroptosis triggers local axon degeneration

While necroptosis induces degeneration via distinct mechanisms in the cell body and the axon, MLKL.ND is dimerized throughout the cell, and so it is not possible to determine whether there is a local axonal necroptotic program or whether the axonal effects are secondary to cell body death. To distinguish between these possibilities, we used microfluidic devices to spatially isolate axons from cell bodies, allowing us to test whether dimerization of MLKL.ND exclusively in axons is sufficient to trigger axon degeneration (Fig. 5 A). Dissociated DRG neurons expressing MLKL.ND were seeded in the somal compartment and extended their axons into the axonal compartment of the microfluidic devices.

To test the hypothesis that necroptosis can occur axon autonomously, we performed three independent experiments. First, addition of the BB dimerizing agent to the axonal side of microfluidic devices was sufficient to induce loss of axonal TMRM staining and local axon degeneration without cell body death. Moreover, this axon degeneration and TMRM loss require SARM1 (Fig. 5, B and C). Hence, local axonal induction of necroptosis in the absence of cell death induces SARM1-dependent axon degeneration. While local axon degeneration is robust in this paradigm, the extent of axon degeneration in microfluidic devices is less dramatic than in normal culture dishes, suggesting that concurrent induction of necroptosis in the soma may contribute to this degenerative event (compare with Fig. 4 C). Second, we observed local calcium influx in axons following axonal-induction of necroptosis. Following axonal application of the BB dimerizer, live-cell imaging revealed a large calcium influx in axons, but not in soma, of WT but not SARM1 KO neurons (Fig. 5 D and Video 2 shows absence of somal calcium influx over time). Taken together, these two experiments show that axonal activation of necroptosis triggers local, SARM1-dependent loss of mitochondrial potential, calcium influx, and axon degeneration.

These studies show that local necroptosis can stimulate the SARM1 degeneration program, but they rely on an engineered system to activate axonal necroptosis. We wondered whether endogenous mechanisms can activate axonal necroptosis in the absence of cell body necroptosis. To test this hypothesis, we asked whether axon-only application of TNF-α could induce local necroptosis as assayed by phosphorylation of MLKL. For immunoblot analysis, microfluidic devices do not provide enough axonal material. Hence, we made spot cultures of SARM1 KO DRG neurons on standard culture dishes, allowed axons to extend, and then removed all cell bodies. Since SARM1 blocks axotomy-induced axon degeneration, these axons remain intact and metabolically healthy for at least 5 d (Geisler et al., 2019b), thus providing adequate time to examine necroptotic signaling. First, we showed that severed axons treated with DMSO for 40 h do not show increases in phosphorylated MLKL (pMLKL), demonstrating that axotomy alone does not increase pMLKL (Fig. 5 E). We then applied TNF-α to these isolated severed axons, collected samples 40 h after TNF-α application, and found that TNF-α triggers an increase in the levels of phosphorylated MLKL that is blocked by the application of necrostatin. Hence, local TNF-α can trigger the necroptotic cascade in axons (Fig. 5 E). This could have important implications for diseases such as multiple sclerosis, where local neuroinflammatory signaling could directly impact axonal health.

Necroptosis depletes axon survival factors

We next investigated the mechanism by which dimerized MLKL.ND activates SARM1 to promote axon degeneration. For axonal maintenance, axon survival factors such as NMNAT2 and SCG10/STMN2 are continuously supplied to the axon to inhibit SARM1 (Gilley et al., 2015; Walker et al., 2017; Shin et al., 2012). Therefore, we tested whether necroptosis decreases NMNAT2 and SCG10 levels in axons. After activation of necroptosis via dimerization of MLKL.ND, axonal NMNAT2 levels significantly decreased over the ensuing 16 h (Fig. 6, A and B). This loss of NMNAT2 only occurs in axons, as there is no change in the levels of somal NMNAT2 (Fig. 6, C and D). Moreover, the levels of axonal SCG10 also decreased after dimerization of MLKL.ND, showing that coregulation of these axon maintenance factors occurs downstream of necroptosis (Fig. 6, C and D). Finally, having demonstrated that endogenous MLKL is required for axon degeneration induced by MLKL.ND dimerization (Fig. S5), we also find that endogenous MLKL is required for the rapid loss of axonal NMNAT2 after dimerization of MLKL.ND (Fig. 6, E and F). Hence, axonal necroptosis triggers the rapid loss of NMNAT2.

SARM1 NAD^+ cleavage activity is required for necroptosis-induced axon degeneration

SARM1 is an inducible NAD^+ cleavage enzyme. During Wallerian degeneration, SARM1 cleaves NAD^+, triggering a metabolic crisis with loss of ATP and subsequent axon degeneration (Fig. 7 A; Sasaki et al., 2020; Essuman et al., 2017; Gerdts et al., 2016). However, SARM1 is also a TLR (Toll-like receptor)-adaptor protein that may participate in traditional innate immune signaling (Mukherjee et al., 2013) separate from its newly found role as an enzyme. Hence, we tested whether this SARM1 NADase activity is required for necroptosis-triggered axon degeneration. First, we assessed the requirement for catalytically active SARM1. The glutamic acid at position 642 is the catalytic residue of the SARM1 NADase, and mutations at position 642 render SARM1 incapable of mediating Wallerian degeneration (Essuman et al., 2017). Here we dimerized MLKL.ND in SARM1 KO neurons expressing GFP, WT SARM1, or the

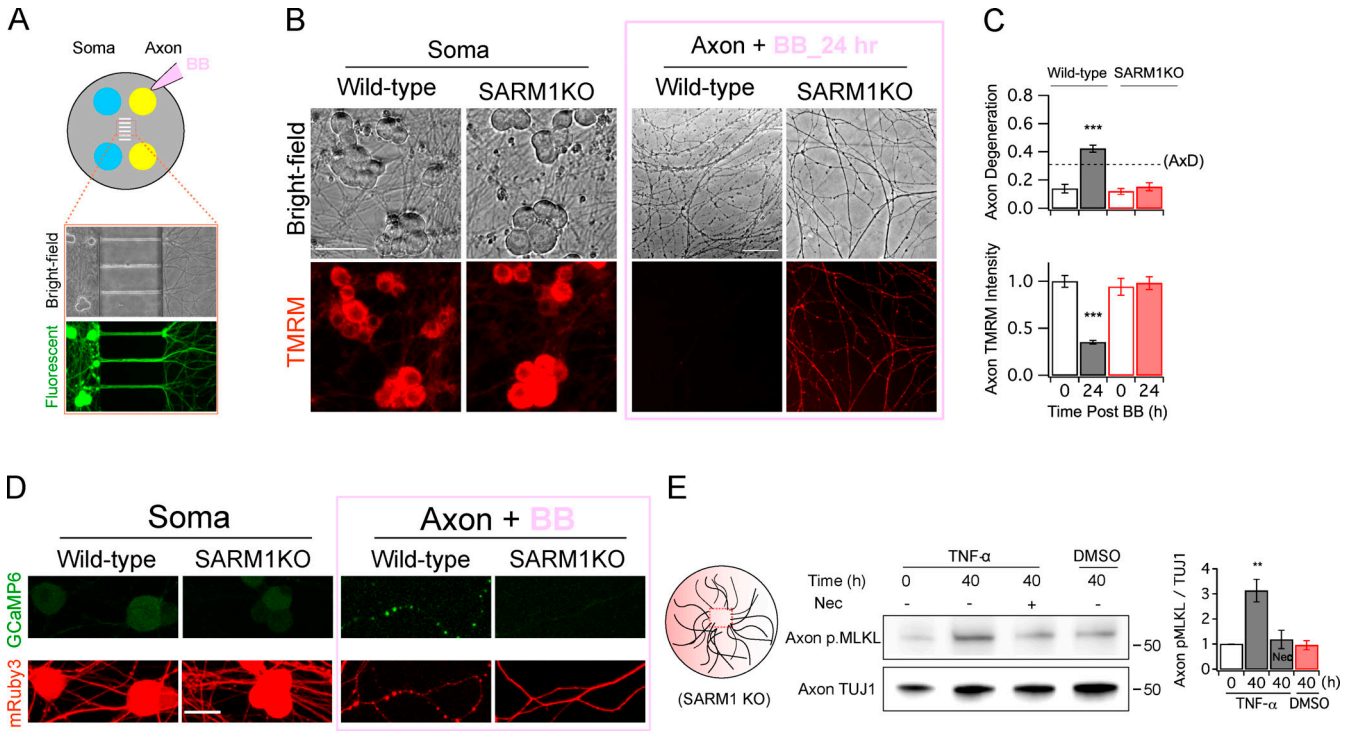

Figure 5. **Axonal necroptosis triggers local axon degeneration. (A)** Schematic diagram of microfluidic device. BB (100 nM) is applied to the axon compartment to dimerize MLKL.ND locally. **(B)** Representative bright-field and TMRM images of soma (left) and axons (right) 24 h after BB is applied to the axon compartment. Scale bar, 50 µm. **(C)** Quantification of axon degeneration (top) and TMRM intensity (bottom). Axons with a DI >0.3 are defined as degenerated (dashed line). Data are represented as mean ± SEM, *n* = 3. For axon degeneration; one-way ANOVA with post hoc Tukey test, F(3, 8) = 29.47, P = 0.0001; for TMRM, one-way ANOVA with post hoc Tukey test, F(3, 8) = 23.28, P = 0.0003; *, P < 0.05; **, P < 0.01; and ***, P < 0.001. **(D)** Representative fluorescent images of soma (left) and axons (right) from WT or SARM1 KO DRG neurons cultured in microfluidic devices. BB is only applied to the axon compartment. Scale bar, 30 µm. **(E)** Left: Schematic of cultured DRGs in which cell bodies have been removed before TNF-α treatment in order to obtain axon-only lysate. Middle: SARM1 KO severed axons are treated with DMSO or TNF-α (100 ng/ml) together with SMAC mimetic (LCL161, 10 µM) and Z.VAD (100 µM) with or without necrostatin-1s (Nec, 20 µM). Axonal extracts are immunoblotted for phosphorylated MLKL. TUJ1 is used as a loading control. Right: Quantification of pMLKL normalized to TUJ1 level. Data represent the mean ± SEM, *n* = 4; one-way ANOVA with post hoc Tukey test, F(2.014, 6.041) = 15.02, P = 0.0045; *, P < 0.05; **, P < 0.01; and ***, P < 0.001. AxD, axon degeneration.

catalytically dead SARM1-E642A. MLKL.ND dimerization triggers axon degeneration only in neurons expressing WT SARM1, demonstrating that catalytically active SARM1 is required for necroptosis-induced axon degeneration (Fig. 7, B and C). Next, we tested whether axon degeneration could be blocked downstream of SARM1 by boosting synthesis of NAD^+ or ATP. During Wallerian degeneration, addition of the NAD^+ precursor nicotinamide riboside (NR) while overexpressing NR kinase (NRK1) increases NAD^+ levels and delays axon degeneration (Sasaki et al., 2016), while incubating neurons with methyl-pyruvate boosts ATP levels (Yang et al., 2015; Cheong et al., 2011). In the presence of NRK1 plus NR or methyl-pyruvate, axon degeneration induced by MLKL.ND dimerization is blocked for at least 24 h. At 48 h, axons are beginning to show minor signs of degeneration (Fig. 7 E). These findings indicate that necroptosis induces a SARM1-dependent metabolic crisis in the axon, and suggest that the mechanisms downstream of SARM1 are likely the same whether SARM1 is activated by axotomy or necroptosis.

Discussion

Our understanding of the molecular mechanisms of neurodegeneration has expanded dramatically with the realization that neuroinflammation contributes to most neurodegenerative diseases (Hammond et al., 2019), that necroptosis is likely as important as apoptosis in driving neuronal cell death (Weinlich et al., 2017; Yuan et al., 2019), and that SARM1 is the central executioner of an axonal self-destruction program activated in diverse neurodegenerative conditions (Figley and DiAntonio, 2020). Here, we unite these disparate degenerative pathways, identifying molecular and functional links among neuroinflammation, necroptosis, and SARM1-mediated axonal self-destruction. These studies support a model in which local neuroinflammatory signals can activate an axonal form of necroptosis that in turns triggers SARM1 NADase activity and axonal demise. These findings have important mechanistic and therapeutic implications for a broad range of neurodegenerative disorders.

SARM1 promotes RGC and oligodendrocyte death in a neuroinflammatory model of glaucoma

While high IOP is the proximate cause of most cases of glaucoma, it is now appreciated that glaucoma is a neurodegenerative disease with a major neuroinflammatory component (Weinreb et al., 2014). Indeed, glaucoma can occur despite normal IOPs, and many patients with high IOP

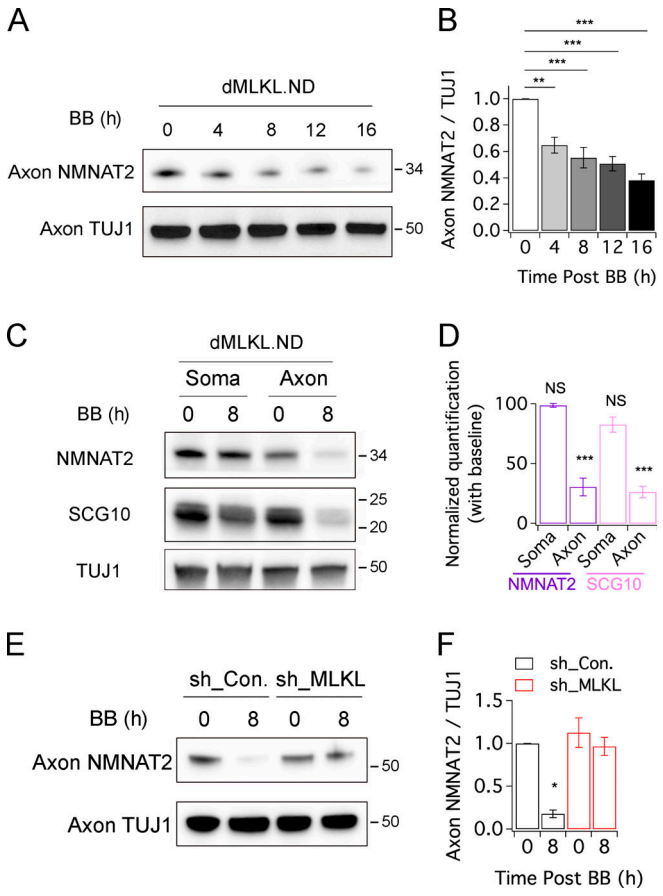

Figure 6. **Axonal necroptosis depletes axon survival factors. (A)** Representative immunoblot of axonal NMNAT2 from WT DRG neurons expressing MLKL.ND at the indicated times following dimerization of MLKL.ND with BB. **(B)** Quantification of axonal NMNAT2 normalized to TUJ1 for the conditions in A. Data represent the mean ± SEM, n = 3 to 4; One-way ANOVA with post hoc Tukey test, $F(4, 12) = 24.51$, $P < 0.0001$; 0 h versus 4 h, $P = 0.0013$; 0 h versus 8 h, $P = 0.0002$; 0 h versus 12 h, $P < 0.0001$; 0 h versus 16 h, $P < 0.0001$; *, $P < 0.05$; **, $P < 0.01$; and ***, $P < 0.001$. **(C)** Immunoblot for the axonal survival factors NMNAT2 and SCG10 from axons and soma of WT DRG neurons expressing MLKL.ND at 0 and 8 h after BB treatment. TUJ1 is used as a loading control. **(D)** Quantification of NMNAT2 and SCG10 levels normalized to TUJ1 from axons or soma 8 h after BB application as described in C. Values are displayed as percentage of 0 h baseline. Data represent the mean ± SEM, n = 4; two-tailed unpaired t test, soma SCG10, $P = 0.065$; axon SCG10, $P = 0.0001$; soma NMNAT2, $P = 0.47$; axon NMNAT2, $P < 0.0001$; NS, not significant; *, $P < 0.05$; **, $P < 0.01$; and ***, $P < 0.001$. **(E)** Representative immunoblot of NMNAT2 in axonal lysates from WT neurons expressing MLKL.ND treated with an shRNA to MLKL or a control shRNA. TUJ1 is used as a loading control. Axonal lysates are collected at baseline and 8 h after BB addition. **(F)** Quantification of axonal NMNAT2 levels normalized to TUJ1 from immunoblots as in E. Data represent the mean ± SEM, n = 3; one-way ANOVA with post hoc Dunnett's multiple comparison test, $F(1.288, 2.575) = 29.26$, $P = 0.0177$; *, $P < 0.05$; **, $P < 0.01$; and ***, $P < 0.001$.

experience continued visual field loss even after restoration of normal pressure (Beidoe and Mousa, 2012). Hence, there is great interest in developing neuroprotective strategies that could be combined with pressure-lowering medications for the treatment and prevention of glaucoma. Here we identify SARM1 as a therapeutic target for neuroprotection in glaucoma.

Using a neuroinflammatory model of glaucoma induced by intravitreal TNF-α injection, we find that SARM1 is required for RGC axon loss and cell death as well as oligodendrocyte loss in the optic nerve. In this system, microglia are activated within days, oligodendrocyte death and RGC axon loss occurs within 2 wk, and ultimately RGC neurons die by 2 mo. Our data demonstrate that SARM1 is not required for microglia activation. Therefore, we suggest that SARM1 functions downstream of neuroinflammatory signaling to promote axonal self-destruction, which in turn promotes oligodendrocyte and RGC death. A variety of results supports the model that axon loss is the driver of oligodendrocyte and RGC death. First, using viral delivery of a neuronally expressed SARM1 dominant-negative transgene provides noncell autonomous protection to oligodendrocytes following TNF-α treatment. Since this oligodendrocyte loss occurs well before RGC death but around the same time as RGC axon loss, it is likely secondary to SARM1-mediated axonal degeneration. Second, while SARM1 can promote neuronal cell death, it does not promote apoptotic cell death (Gerdts et al., 2013; Summers et al., 2014), the likely mechanism of RGC death in glaucoma (Syc-Mazurek and Libby, 2019). Indeed, inhibiting apoptosis blocked RGC death in the DBA/2 chronic glaucoma model, but failed to protect optic nerve axons (Libby et al., 2005). In contrast, following optic nerve transection, SARM1 KO blocks degeneration of the severed distal axons, but does not protect against cell body death, which instead is mediated by retrograde axonal signals that activate apoptosis (Welsbie et al., 2013; Simon and Watkins, 2018; Syc-Mazurek and Libby, 2019). The different requirements for SARM1 following optic nerve transection and TNF-α application are instructive. Transection directly disrupts axons, thereby triggering retrograde apoptotic signals, while with TNF-α treatment, SARM1-induced axon degeneration is the cause of the axon loss that likely activates the apoptotic signals. Hence, by inhibiting SARM1, axons are protected and secondary apoptotic signaling is prevented.

A role for SARM1 in glaucoma may explain the mechanism of metabolic dysfunction in glaucomatous optic nerves. In DBA/2J, ATP levels in optic nerve are dramatically reduced at 6 mo, well before optic nerve loss (Baltan et al., 2010; Inman and Harun-Or-Rashid, 2017; Libby et al., 2005; Howell et al., 2007). SARM1 is an inducible NAD^+ cleaving enzyme, and SARM1 activation induces axonal NAD^+ loss that is followed by ATP loss, likely due to the central role of NAD^+ in both oxidative phosphorylation and glycolysis (Essuman et al., 2017; Gerdts et al., 2016). If neuroinflammation induces low-level SARM1 activation, this may trigger metabolic vulnerability of glaucomatous optic axons and explain the protective effects of NAD^+ supplementation (Kitaoka et al., 2009; Williams et al., 2017b) and overexpression of the NAD biosynthetic enzyme NMNAT in many (Howell et al., 2007; Kitaoka et al., 2009; Williams et al., 2017a; Zhu et al., 2013), but not all, glaucoma models (Beirowski et al., 2008).

TNF-α is up-regulated in the vitreous, retina, and optic nerves of glaucoma patients (Yan et al., 2000; Sawada et al., 2010; Tezel et al., 2001; Huang et al., 2010) as well as in response to increased IOP in rodent models (Roh et al., 2012; Nakazawa et al., 2006; Cueva Vargas et al., 2015). Pharmacological

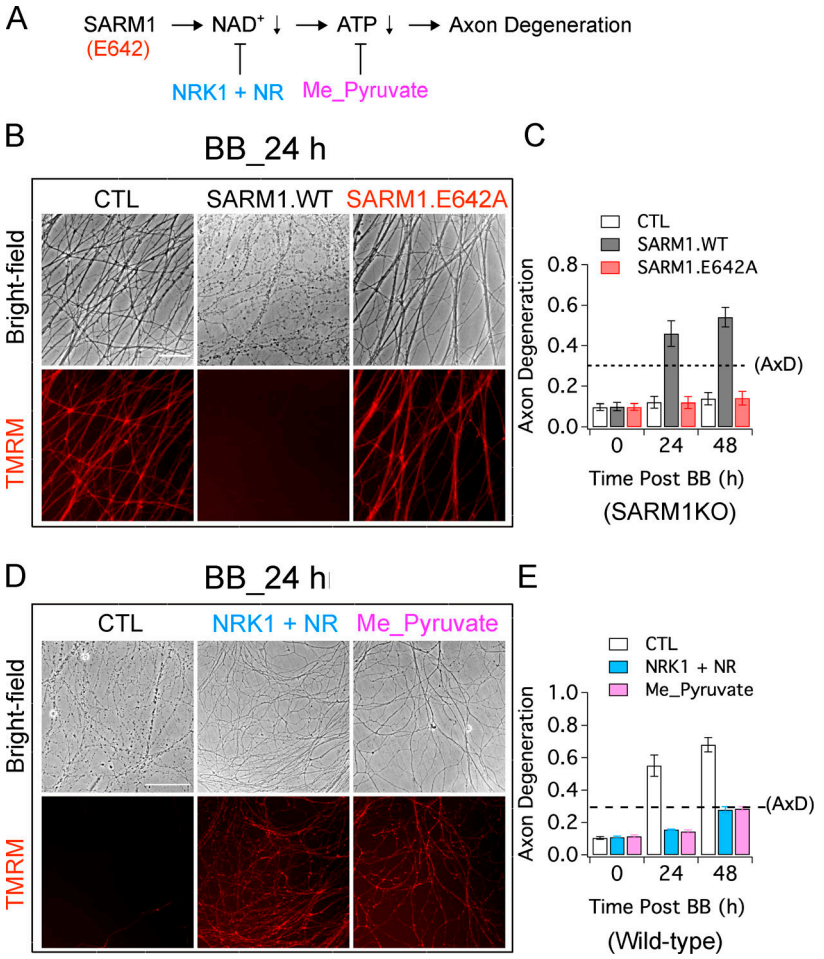

Figure 7. **SARM1 NADase activity is required for necroptosis-induced axon degeneration. (A)** Schematic diagram of interventions that impact SARM1-mediated axon degeneration. Glutamic acid 642 (E642) is the catalytic residue of the SARM1 NADase. NRK1 + NR promote NAD^+ synthesis. Methyl pyruvate (Me_Pyruvate) promotes ATP synthesis. **(B)** Representative bright-field and TMRM images of axons of SARM1 KO DRG neurons expressing MLKL.ND at 24 h after BB application. SARM1 KO neurons expressing MLKL.ND are infected with lentivirus expressing either GFP as a control (CTL), WT SARM1 (SARM1.WT), or catalytically dead SARM1 (SARM1.E642A). Scale bar, 50 µm. **(C)** Quantitative analysis of axon degeneration at the indicated times after BB (100 nM) application from bright-field images for the conditions described in B. Axons with a DI >0.3 are defined as degenerated (dashed line). Data represent the mean ± SEM, $n = 4$; two-way ANOVA with post hoc Bonferroni's multiple comparison test; time, $F(1.472, 13.25) = 102.7$, $P < 0.0001$; interaction, $F(9, 18) = 12.88$, $P < 0.0001$; *, $P < 0.05$; **, $P < 0.01$; and ***, $P < 0.001$. **(D)** Representative bright-field and TMRM images of axons of WT DRG neurons expressing MLKL.ND 24 h after BB addition. Neurons are treated with 1 mM NR while infected with lentivirus expressing NRK1, 5 mM Me_Pyruvate, or no addition (CTL, control). Scale bar, 100 µm. **(E)** Quantitative analysis of axon degeneration at the indicated times after BB addition from bright-field images for the conditions described in D. Axons with a DI >0.3 are defined as degenerated (dashed line). Data represent the mean ± SEM, $n = 3$; two-way ANOVA with post hoc Bonferroni's multiple comparison test; time, $F(1.472, 13.25) = 102.7$, $P < 0.0001$; interaction, $F(9, 18) = 12.88$, $P < 0.0001$; *, $P < 0.05$,; **, $P < 0.01$; and ***, $P < 0.001$.

and genetic manipulation of TNF-α signaling demonstrates that it promotes microglial activation, yet how that ultimately triggers RGC axon loss and death remains unknown. Here we show that TNF-α application rapidly induces the up-regulation and phosphorylation of RIPK3 and MLKL in optic nerve, consistent with induction of necroptosis. We also show that TNF-α–dependent loss of oligodendrocytes, RGC axons, and RGC cell bodies is SARM1-dependent. These data, in conjunction with prior studies in glaucoma, are consistent with a model in which increases in IOP trigger TNF-α release, which in turn activates microglia, initiating a positive feedback loop that leads to further release of damaging cytokines. These inflammatory factors may then act on RGC axons to trigger an axonal form of necroptosis that activates SARM1 NADase activity. Accordingly, activated SARM1 would impair RGC axonal metabolism and promote axon degeneration and loss of associated oligodendrocytes. Once the axon is disconnected from its target, retrograde apoptotic signals would promote death of RGCs. If this model were correct, then pharmacological or gene therapy approaches to inhibit SARM1 would be neuroprotective in glaucoma, maintaining axonal integrity and blocking downstream death of oligodendrocytes and RGCs. Moreover, such a mechanism is unlikely to be limited to the eye, and may be broadly relevant to neurodegenerative diseases associated with neuroinflammation.

Axonal necroptosis triggers SARM1-dependent axon degeneration

In classical Wallerian degeneration, the mechanism of SARM1-dependent axon degeneration is well understood. In a healthy axon, SARM1 is held inactive via inhibition by the axonal survival factors NMNAT2 and SCG10/STMN2. Both NMNAT2 and SCG10 are labile with very short half-lives, and so they must be constantly replenished in the axon via fast axonal transport. Upon axotomy, no new NMNAT2 or SCG10 can be delivered to the distal axon, and levels of these axon survival factors consequently drop, allowing stimulation of SARM1 NADase activity and triggering a metabolic crisis and axonal degeneration. A similar mechanism is thought to occur in response to neurotoxic chemotherapeutics such as vincristine, which disrupt axonal transport without a frank transection, and so would be expected to reduce NMNAT2 and SCG10 at the most distal portion of the axon. This likely explains the distal dying-back pathology that is a hallmark of peripheral neuropathy. Here, we greatly expand the reach of this model for SARM1 activation, demonstrating that neuroinflammatory and necroptotic signaling in the axon reduces the levels of the axonal survival factors NMNAT2 and SCG10 and triggers SARM1-dependent axonal degeneration. Since neuroinflammation and necroptosis are major contributors to a broad range of neurodegenerative diseases, and since axon degeneration is an early and major contributor to neuropathology

in many of these disorders, we hypothesize that the molecular links identified here among neuroinflammation, necroptosis, and SARM1 activity are important mediators of axon loss in these diseases.

Here, we provide evidence for a specialized form of necroptosis that works in the axon through SARM1 to promote axon degeneration. First, we show that TNF-α stimulates necrostatin- and SARM1-dependent axon degeneration, and find that TNF-α application exclusively to axons triggers necroptosis as assayed by phosphorylation of MLKL. Hence, the machinery for necroptosis is present in the axons. Second, we demonstrate that direct activation of necroptosis via dimerization of MLKL.ND works through endogenous MLKL to trigger mechanistically distinct degenerative outcomes in the axon versus cell body. In the cell body, dimerized MLKL.ND induces calcium influx and cell death that is SARM1-independent, which is consistent with the canonical role for MLKL as an inducer of membrane permeabilization, either directly via forming a pore or through activation of TRPM7 channels (Cai et al., 2014; Xia et al., 2016). In the axon, however, dimerized MLKL.ND requires SARM1 to trigger calcium influx and axon degeneration, implying that axonal MLKL is not sufficient to disrupt membranes. This is a very surprising finding given the "pore forming" function of MLKL in canonical necroptosis. Instead, we show that dimerized MLKL.ND and endogenous MLKL promote the loss of the axon survival factors NMNAT2 and SCG10. Once axonal necroptosis lowers levels of these survival factors, the mechanism of axon degeneration is similar to that observed for Wallerian degeneration. Whether triggered by axonal necroptosis or axotomy, axon loss requires SARM1 NADase activity, is blocked by overexpression of cytoplasmic NMNAT1 or inhibition of the DLK/LZK stress kinases, and involves metabolic catastrophe that can be rescued via supplementation with NAD^+ and ATP precursors.

How might axonal necroptosis trigger loss of the axonal survival factors NMNAT2 and SCG10? The finding that axonal necroptosis coregulates both factors is a clue, as we have previously demonstrated that palmitoylated forms of NMNAT2 and SCG10 colocalize to axonal vesicles, and are coregulated by DLK/LZK working through a JNK neuronal stress pathway (Summers et al., 2018). JNK activity promotes the turnover of both NMNAT2 and SCG10. Interestingly, necroptosis can also stimulate JNK activation (McNamara et al., 2013; Gautheron et al., 2014), and hence this could be a mechanism by which necroptosis stimulates SARM1-dependent axon degeneration.

There is controversy about whether or not necroptosis contributes to traditional Wallerian degeneration. Yang et al. (2015) reported that inhibiting necroptosis does not influence axotomy-induced Wallerian degeneration, but a recent study from Arrázola et al. (2019) claimed that axotomy activates necroptosis and promotes Wallerian degeneration. Our results are consistent with previous findings (Yang et al., 2015), as we do not see activation of necroptosis in response to axotomy, and neither genetic nor pharmacological inhibition of necroptosis blocks axotomy-induced axon degeneration (Fig. S8). However, the recent findings that necroptosis promotes axon degeneration in both excitotoxicity and Parkinson's models (Hernández et al., 2018; Oñate et al., 2020) are consistent with the findings reported here, although the role of the SARM1 pathway was not explored in those studies.

Here, we identify a central role for SARM1 in promoting axon, RGC, and oligodendrocyte loss in glaucoma. Major efforts are underway to develop pharmacological and gene therapy approaches to inhibit SARM1 (DiAntonio, 2019), and hence SARM1 is a realistic therapeutic target for neuroprotection in glaucoma. In addition, we identify a specialized form of axonal necroptosis that links neuroinflammation to SARM1-dependent axon degeneration. This unification of three major neurodegenerative mechanisms has broad implications for the pathogenesis and treatment of a wide range of neurodegenerative disorders. This finding may be of particular interest in diseases such as multiple sclerosis, where neuroinflammation may directly impact the axon.

Materials and methods

Further information about resources and materials is listed in Table S1.

Animals

All procedures were performed in accordance with guidelines mandated in the National Institutes of Health Guide for the Care and Use of Laboratory Animals and approved by the Washington University School of Medicine in St. Louis Institutional Animal Care and Use Committee. C57BL/6 mice were purchased from Jackson Laboratory, and SARM1KO mice were a gift from M. Colonna at Washington University in St. Louis (Szretter et al., 2009). CD1 mice (gestation day 11.5) for sensory neuron cultures was purchased from Charles River Laboratories.

Intravitreal injection

2 µl TNF-α (1 ng in 1 µl of PBS with 0.1% BSA) or PBS was injected into the vitreous chamber of one eye of 5-wk-old mice (WT or SARM1 KO) using a syringe pump (Harvard Apparatus 22 syringe pump; Harvard Apparatus). A 33-gauge beveled needle (NanoFil) is used for 5-wk-old mice. Given that the vitreous volume is ∼10 µl (Remtulla and Hallett, 1985; Sharma et al., 2005; Yu and Cringle, 2006), the concentration of TNF-α is ∼0.2 mg/ml. Only one eye was injected with TNF-α or PBS for experiments. The needle tip with 45° angle was slowly inserted into the vitreous body through the sclera of the superior hemisphere of the eye. The speed of the injection is 7.5 µl/min. If eyes are damaged resulting in retinal detachment or bleeding, and/or iris/lens injury, then those eyes were excluded for data analysis because previous studies have shown that eye injury releases neuronal survival factors (Fischer et al., 2001; Leon et al., 2000).

AAV constructs and virus injection

AAV vector expressing EGFP (pAAV-hSyn-EGFP) was obtained from Addgene (gift from B. Roth, School of Medicine at the University of North Carolina at Chapel Hill, Chapel Hill, NC; Addgene 50465). This vector was cut with BamHI and NcoI, and then SARM1.WT or SARM1-K193R/H194A/H685A (SARM1.DN) was inserted between the synapsin promoter and EGFP

sequence using in-Fusion HD Cloning kit (Clontech; Geisler et al., 2019b). In the retina, viral expression driven by the synapsin promoter is weaker than that of the commonly used nonneuronal promoter chicken-b-actin promoter with cytomegalovirus enhancer, so we used a capsid mutant, 7m8, to overcome tissue penetration for gene delivery (Yin et al., 2011; Dalkara et al., 2013). This virus is delivered with intravitreal injection like TNF-α injection.

DRG neurons culture/experimental timeline

Mouse DRG neurons were dissected from embryonic days 13.5 or 14.5 from CD1 mouse embryos. DRG neurons were incubated with 0.05% trypsin containing 0.02% EDTA at 37°C for 20 min and then resuspended in neurobasal media (Gibco) containing 2% B27 (Invitrogen), 50 ng/ml nerve growth factor (Harlan Laboratories), 1 µM 5-fluoro-2deoxyuridine (Sigma-Aldrich), 1 µM uridine (Sigma-Aldrich), and penicillin/streptomycin (Thermo Fisher Scientific). The dissociated DRG neurons were plated in 24-well or 96-well plates (Corning) coated with poly-D-lysine (0.1 mg/ml; Sigma-Aldrich) and laminin (3 µg/ml; Invitrogen) and then allowed to adhere in humidified tissue culture incubator (5% CO_2) for 15 min. Finally, DRG growth medium was gently added (500 µl for 24-well, 100 µl for 96-well). Lentivirus was transduced at 1 or 2 d in vitro (DIV). At DIV7, assays for axon degeneration and/or cell death were performed by applying BB (or TNF-α) or axotomy.

Lentivirus construction/production

The following murine MLKL-specific (target sequence: 5′-GAG ATCCAGTTCAACGATA-3′) shRNA was engineered using two primers (Integrated DNA Technologies) that were annealed, phosphorylated, and ligated into AgeI and EcoRI restriction sites of pLKO.1 vector: shMLKL (5′-CCGGTGGAGATCCAGTTCAAC GATATTCAAGAGATATCGTTGAACTGGATCTCTTTTTTG-3′, and 5′-AATTCAAAAAAGAGATCCAGTTCAACGATATCTCTTGAA TATCGTTGAACTGGATCTCCA-3′). GCaMP6f (Addgene 72303) and mRuby3 (Addgene 74252) were amplified by PCR and ligated into BamHI and EcoRI restriction sites of FCIV lentiviral vector (Araki et al., 2004) using homologous recombination-based InFusion system (Clontech): GCaMP6 (forward: 5′-GACTCTAGA GGATCCGCCACCATGGGTTCTCATCATCATCAT-3′, reverse: 5′-CTTGATATCGAATTCTCACTTCGCTGTCATCATTTG-3′), mRuby3 (forward: 5′-GACTCTAGAGGATCCGCCGCCACCATGGTGTCTAAG GGCGAAGAGCTG-3′, reverse: 5′-CTTGATATCGAATTCTTACTT GTACAGCTCGTCCAT-3′). MLKL.ND (Human ORF Library, CloneID: TOLH-1510032, Tissue Culture Support Center, Washington University in St. Louis) were amplified by PCR and ligated into BsiWI and EcoRI restriction sites of FCIV-Fkbp^{F36V}-TIR (Gerdts et al., 2015): MLKL.ND (forward: 5′-AAACTGGAATCGTACGCGTCC CGGGGCGGTGGCTCATCTGGCGGAGGTATGGAAAATTTGAAG CATATT-3′; reverse: 5′-GCTTGATATCGAATTCCTACTGCCTCAA AGTTTCCTTGAT-3′).

HEK293T cells were used for lentivirus production (Araki et al., 2004). Cells were seeded at 70–80% confluency per 35-mm well the day before transfection. FCIV or shRNA lentivirus constructs (1.2 µg) were cotransfected with vesicular stomatitis virus - G (600 ng) and pSPAX2 (800 ng) using FuGENE 6 (Promega). The lentiviral supernatants were collected at 2 d after transfection, and then the cleared supernatant was concentrated with Lenti-X Concentrator (Clontech) to a final concentration of 1–10 × 10^7 particles/ml. Lentivirus transduction efficiency was monitored with tagged fluorophore and is ∼100% in DRG neurons. There is no difference in expression level between WT and SARM1 KO DRG neurons.

Live-cell imaging of axonal calcium

DRG neurons were cultured in a FluoroDish (WPI) that has a glass bottom, allowing for use of an objective lens with immersion oil for GCaMP6 calcium imaging. At DIV2, lentivirus expressing GCaMP6 for calcium and mRuby3 for axon integrity were transduced to cultured DRG neurons. To maintain 37°C temperature, and 100 ml/min 5% CO_2/95% airflow rate during imaging, a Chamlide TC (Live Cell Instrument) was connected to a Leica DMI4000B microscope under confocal settings using 20× oil immersion objectives (NA 0.6) and Leica DFC7000 T 2.8 MP Color Microscope Camera at RT. The Leica Application Suite X is the software platform to acquire and analyze images. Optical sectioning and laser settings were kept constant across all image data acquisition sessions. Images for GCaMP6 and mRuby3 were acquired every 30 or 60 min until the end of the imaging session.

Immunohistochemistry

Retina and optic nerves were fixed with 4% PFA for 2 h at RT. Blocking solution was made with PBS including 10% normal goat serum and 0.3% TX-100. The primary and secondary antibodies were diluted in blocking solution and incubated at 4°C for overnight. Antibodies include mouse anti-Brn3a (1:100, Santa Cruz, Sc-8429), rabbit anti-Iba1 (1:1,000, Wako, 019–19741), mouse anti-CC1 (1:500, Millipore Sigma-Aldrich, OP80), and mouse (BioLegend, 801202) or rabbit (Millipore Sigma-Aldrich, T3952) anti-TUJ1 (1:1,000). The following day, Alexa Fluor–conjugated secondary antibodies were incubated for 2 h at RT (Table S1). Tissue samples were mounted in Vectashield (with DAPI) for visualization with a Leica DMI4000B microscope under confocal settings. For the 16-µm tissue sections of retina or optic nerve (Fig. S1), a cryostat (Leica CM1860) was used.

Western blot analysis

Lysate buffers contain protease (cOmplete, mini, EDTA-free protease inhibitor cocktail) and phosphatase inhibitor (PhosSTOP). The lysate buffers were preferentially selected for different proteins. While radioimmunoprecipitation assay buffer was preferentially used for detecting MLKL and phosphorylated MLKL proteins, Laemmli buffer was specifically used for detecting NMNAT2 and SCG10. Other proteins have no preference. Lysates were precleared of debris by centrifugation at 10,000 *g* in a refrigerated microcentrifuge for 10 min. Supernatants were mixed with 5% 2-mercaptoethanol (Millipore Sigma-Aldrich) and then boiled for 10 min. Finally, clarified extracts were mixed with Laemmli buffer (60 mM Tris-HCl, pH 6.8, 50% glycerol, 2% SDS, and 0.1% bromophenol blue) and analyzed by SDS/PAGE and Western blotting. TBS-T (TBS and 0.2% Tween 20) was used to wash immunoblots in all procedures. For blocking buffers, 5% milk was commonly added to TBS-T. However, for detecting

phosphorylated MLKL proteins, 5% BSA was specifically used instead of milk. After 1 h block at RT, the membrane was incubated overnight with primary antibody. Primary antibodies were diluted in the blocking buffer as follows: rabbit anti-pMLKL (1:1,000, S345, Abcam, Ab196436), rabbit anti-MLKL (1:500, abcepta, AP14272B), rabbit anti-RIP3 (1:500, Abcam, ab56164), rabbit anti-pRIP3 (T231/S232, 1:500, Cell Signaling, 57220), mouse anti-TUJ1 (1:1,000, BioLegend, 801202), rabbit anti-caspase 3 (1:1,000, Cell Signaling, 9962), rabbit anti-cleaved caspase 3 (1:500, Cell Signaling, 9661), mouse anti-NMNAT2 (1:100, Santa Cruz, Sc-515206), and rabbit anti-SCG10 (1:2,000, Proteintech Group). The following day, HRP-conjugated anti-mouse or anti-rabbit secondary antibodies (1:5,000 or 1:10,000, Jackson ImmunoResearch; 115–035-003 or 111–035-144) were incubated for 1 h. For developing immunoblots, a chemiluminescent method (Millipore Sigma-Aldrich) was used. TUJ1 was used in all experiments as a loading control. All data quantification of immunoblots was performed with ImageJ.

Optic nerves

3 d after TNF-α or PBS injection, optic nerves were collected and homogenized with cold radioimmunoprecipitation assay buffer. Homogenization of optic nerves was repeated three times every 20 min on ice.

Axons from DRG neurons

To acquire axon-only lysates, dense spot cultures were prepared in 24-well plates. Due to the high density of DRG neurons, half media changes are made every 3 d to prevent nutrient loss. On DIV7, a plate was placed first on ice, and then washed with a cold PBS several times. A microscalpel was used to remove cell bodies of DRG neurons (Fig. S8 A and Fig. 5 E). Axon-only lysate was collected from three or four wells.

Data analysis

Retina and optic nerve

In each experiment, sample number (*n*) indicates the number of animals in vivo, and the number of embryos in vitro. At least five EM pictures per optic nerve were randomly imaged, and then analyzed/averaged from one animal (Fig. 1, C–E; and Fig. 2 E). To count Brn3a-positive neurons (Fig. 1 G) and Iba1-positive microglia (Fig. 2 B), three pictures of the retina near optic nerve head were acquired and analyzed from each animal. For quantification of CC1-positive oligodendrocytes after TNF-α injection (Fig. 2, D and H), three to four cross-sections (16-µm thickness/section) of the proximal optic nerve regions were obtained from a distance of ∼1 mm behind the eye. Those three to four sections from one optic nerve were analyzed, and then averaged as $n = 1$. When counting the number of CC1-positive oligodendrocytes, the staining that overlaid with nuclear staining was considered specific.

Axon degeneration

The axon degeneration index (DI) at baseline should be <0.2 to define intact axons. If baseline measurements were >0.2, we did not further process experiments as this is an indication of an unhealthy neuronal culture. In this study, if the axon DI is >0.3 after treatment, then we define those axons as degenerated. As values increase beyond 0.3, the axons tend to have smaller axonal fragments remaining.

Cell death

To define cell death, we used DAPI (or Hoechst) and EthD (or propidium iodide [PI]). In general, nuclei of dead cells only stain for EthD (or PI), and do not stain for DAPI (or Hoechst). The percentage of cell death is calculated by EthD staining / (EthD staining + DAPI staining) × 100.

Neuron-specific expression of AAV-SARM1.DN

To confirm that AAV-SARM1.DN is not expressed in oligodendrocyte (Fig. S1, C and D), single-section images of four different channels of a confocal microscope were acquired for the analysis of pixel intensity. As seen in Fig. S1 C, one line is drawn in a merged image, and then intensity is measured of each pixel for four different channels. The intensity of pixels is plotted in Fig. S1 D. In this example, because the peak of CC1 pixel (red) is far from the peak of SARM1.DN (green), we are able to define that SARM1.DN is not expressed in oligodendrocytes.

Statistical analyses

All statistics were performed with GraphPad Prism 8 software. The Shapiro–Wilk test was used for normality whether or not data assumed a Gaussian distribution. To determine statistical significance between groups, unpaired two-way Student's *t* test, one-way ANOVA with post hoc Tukey test, or two-way ANOVA with post hoc Bonferroni's multiple comparison test were used (detailed in figure legends). Statistical significance was noted as *, $P < 0.05$; **, $P < 0.01$; and ***, $P < 0.001$. All error bars represent mean ± SEM.

Online supplemental material

Fig. S1 shows that intravitreal injection of AAV-hSyn-SARM1.DN-EGFP drives expression in RGCs but not oligodendrocytes. Fig. S2 shows that cleaved caspase 3 is not detected in the optic nerve of TNF-α–injected eyes. Fig. S3 shows that necrostatin-1s does not prevent axon degeneration following dimerization of MLKL.ND. Fig. S4 shows validation of shRNA for MLKL in cultured DRG neurons and N2a cells. Fig. S5 shows that dimerized MLKL.ND requires endogenous MLKL to induce axon degeneration. Fig. S6 shows that SARM1 KO does not prevent cell death induced by dimerization of MLKL.ND. Fig. S7 shows that DLK inhibition and cytoNMNAT1 expression block axon degeneration induced by dimerization of MLKL.ND. Fig. S8 shows that necroptosis is not activated by or required for Wallerian degeneration. Table S1 shows reagents used in the study. Video 1 shows that calcium influx by dimerization of MLKL.ND is completely prevented in axons from SARM1 KO neurons. Video 2 shows local calcium influx in axons, not in soma by dimerization of MLKL.ND.

Acknowledgments

We thank members of the DiAntonio and Milbrandt laboratories for fruitful discussions. In particular, we thank Amy Strickland

and Wandy Beatty for tissue processing of optic nerves and EM. AAV capsid 7m8 was a kind gift from J. Flannery and D. Schaffer (University of California, Berkeley, Berkeley, CA).

This work was supported by National Institutes of Health grants R01CA219866, and RO1NS087632 (to J. Milbrandt and A. DiAntonio), and RF1-AG013730 (to J. Milbrandt) and the Hope Center Viral Vector Core at the Washington University School of Medicine in St. Louis.

A. DiAntonio, J. Milbrandt, and Washington University are inventors on patents related to this work. A. DiAntonio and J. Milbrandt are cofounders of Disarm Therapeutics, and A. DiAntonio and J. Milbrandt are members of its scientific advisory board. The remaining author declares no competing financial interests.

Author contributions: K.W. Ko and A. DiAntonio designed the research. K.W. Ko performed all research and data analysis. K.W. Ko, J. Milbrandt, and A. DiAntonio wrote the manuscript. J. Milbrandt and A. DiAntonio supervised experiments.

Submitted: 9 December 2019
Revised: 8 April 2020
Accepted: 27 April 2020

References

Almasieh, M., A.M. Wilson, B. Morquette, J.L. Cueva Vargas, and A. Di Polo. 2012. The molecular basis of retinal ganglion cell death in glaucoma. *Prog. Retin. Eye Res.* 31:152–181. https://doi.org/10.1016/j.preteyeres.2011.11.002

Araki, T., Y. Sasaki, and J. Milbrandt. 2004. Increased nuclear NAD biosynthesis and SIRT1 activation prevent axonal degeneration. *Science.* 305: 1010–1013. https://doi.org/10.1126/science.1098014

Arrázola, M.S., C. Saquel, R.J. Catalán, S.A. Barrientos, D.E. Hernandez, N.W. Martínez, A. Catenaccio, and F.A. Court. 2019. Axonal Degeneration Is Mediated by Necroptosis Activation. *J. Neurosci.* 39:3832–3844. https://doi.org/10.1523/JNEUROSCI.0881-18.2019

Bajar, B.T., E.S. Wang, A.J. Lam, B.B. Kim, C.L. Jacobs, E.S. Howe, M.W. Davidson, M.Z. Lin, and J. Chu. 2016. Improving brightness and photostability of green and red fluorescent proteins for live cell imaging and FRET reporting. *Sci. Rep.* 6:20889. https://doi.org/10.1038/srep20889

Baltan, S., D.M. Inman, C.A. Danilov, R.S. Morrison, D.J. Calkins, and P.J. Horner. 2010. Metabolic vulnerability disposes retinal ganglion cell axons to dysfunction in a model of glaucomatous degeneration. *J. Neurosci.* 30:5644–5652. https://doi.org/10.1523/JNEUROSCI.5956-09.2010

Beidoe, G., and S.A. Mousa. 2012. Current primary open-angle glaucoma treatments and future directions. *Clin. Ophthalmol.* 6:1699–1707. https://doi.org/10.2147/OPTH.S32933

Beirowski, B., E. Babetto, M.P. Coleman, and K.R. Martin. 2008. The WldS gene delays axonal but not somatic degeneration in a rat glaucoma model. *Eur. J. Neurosci.* 28:1166–1179. https://doi.org/10.1111/j.1460-9568.2008.06426.x

Bosco, A., M.R. Steele, and M.L. Vetter. 2011. Early microglia activation in a mouse model of chronic glaucoma. *J. Comp. Neurol.* 519:599–620. https://doi.org/10.1002/cne.22516

Büning, H., and A. Srivastava. 2019. Capsid Modifications for Targeting and Improving the Efficacy of AAV Vectors. *Mol. Ther. Methods Clin. Dev.* 12: 248–265. https://doi.org/10.1016/j.omtm.2019.01.008

Caccamo, A., C. Branca, I.S. Piras, E. Ferreira, M.J. Huentelman, W.S. Liang, B. Readhead, J.T. Dudley, E.E. Spangenberg, K.N. Green, et al. 2017. Necroptosis activation in Alzheimer's disease. *Nat. Neurosci.* 20:1236–1246. https://doi.org/10.1038/nn.4608

Cai, Z., S. Jitkaew, J. Zhao, H.C. Chiang, S. Choksi, J. Liu, Y. Ward, L.G. Wu, and Z.G. Liu. 2014. Plasma membrane translocation of trimerized MLKL protein is required for TNF-induced necroptosis. *Nat. Cell Biol.* 16:55–65. https://doi.org/10.1038/ncb2883

Chen, T.-W., T.J. Wardill, Y. Sun, S.R. Pulver, S.L. Renninger, A. Baohan, E.R. Schreiter, R.A. Kerr, M.B. Orger, V. Jayaraman, et al. 2013. Ultrasensitive fluorescent proteins for imaging neuronal activity. *Nature.* 499:295–300. https://doi.org/10.1038/nature12354

Cheong, J.-H., E.S. Park, J. Liang, J.B. Dennison, D. Tsavachidou, C. Nguyen-Charles, K. Wa Cheng, H. Hall, D. Zhang, Y. Lu, et al. 2011. Dual inhibition of tumor energy pathway by 2-deoxyglucose and metformin is effective against a broad spectrum of preclinical cancer models. *Mol. Cancer Ther.* 10:2350–2362. https://doi.org/10.1158/1535-7163.MCT-11-0497

Coleman, M.P., and A. Höke. 2020. Programmed axon degeneration: from mouse to mechanism to medicine. *Nat. Rev. Neurosci.* 21:183–196. https://doi.org/10.1038/s41583-020-0269-3

Cueva Vargas, J.L., I.K. Osswald, N. Unsain, M.R. Aurousseau, P.A. Barker, D. Bowie, and A. Di Polo. 2015. Soluble Tumor Necrosis Factor Alpha Promotes Retinal Ganglion Cell Death in Glaucoma via Calcium-Permeable AMPA Receptor Activation. *J. Neurosci.* 35:12088–12102. https://doi.org/10.1523/JNEUROSCI.1273-15.2015

Dalkara, D., L.C. Byrne, R.R. Klimczak, M. Visel, L. Yin, W.H. Merigan, J.G. Flannery, and D.V. Schaffer. 2013. In Vivo-Directed Evolution of a New Adeno-Associated Virus for Therapeutic Outer Retinal Gene Delivery from the Vitreous. *In* Sci. Transl. Med. Vol. 5. p. 189ra76. https://doi.org/10.1126/scitranslmed.3005708

Davis, B.M., M. Salinas-Navarro, M.F. Cordeiro, L. Moons, and L. De Groef. 2017. Characterizing microglia activation: a spatial statistics approach to maximize information extraction. *Sci. Rep.* 7:1576. https://doi.org/10.1038/s41598-017-01747-8

DiAntonio, A.. 2019. Axon degeneration: mechanistic insights lead to therapeutic opportunities for the prevention and treatment of peripheral neuropathy. *Pain.* 160(Suppl 1):S17–S22. https://doi.org/10.1097/j.pain.0000000000001528

Do, Y.J., J.W. Sul, K.H. Jang, N.S. Kang, Y.H. Kim, Y.G.H. Kim, and E. Kim. 2017. A novel RIPK1 inhibitor that prevents retinal degeneration in a rat glaucoma model. *Exp. Cell Res.* 359:30–38. https://doi.org/10.1016/j.yexcr.2017.08.012

Essuman, K., D.W. Summers, Y. Sasaki, X. Mao, A. DiAntonio, and J. Milbrandt. 2017. The SARM1 Toll/Interleukin-1 Receptor Domain Possesses Intrinsic NAD^+ Cleavage Activity that Promotes Pathological Axonal Degeneration. *Neuron.* 93:1334–1343.e5. https://doi.org/10.1016/j.neuron.2017.02.022

Fegan, A., B. White, J.C.T. Carlson, and C.R. Wagner. 2010. Chemically controlled protein assembly: techniques and applications. *Chem. Rev.* 110: 3315–3336. https://doi.org/10.1021/cr8002888

Fernandes, K.A., K.L. Mitchell, A. Patel, O.J. Marola, P. Shrager, D.J. Zack, R.T. Libby, and D.S. Welsbie. 2018. Role of SARM1 and DR6 in retinal ganglion cell axonal and somal degeneration following axonal injury. *Exp. Eye Res.* 171:54–61. https://doi.org/10.1016/j.exer.2018.03.007

Figley, M.D., and A. DiAntonio. 2020. The SARM1 axon degeneration pathway: control of the NAD^+ metabolome regulates axon survival in health and disease. *Curr. Opin. Neurobiol.* 63:59–66. https://doi.org/10.1016/j.conb.2020.02.012

Fischer, D., P. Heiduschka, and S. Thanos. 2001. Lens-injury-stimulated axonal regeneration throughout the optic pathway of adult rats. *Exp. Neurol.* 172:257–272. https://doi.org/10.1006/exnr.2001.7822

Fuchs, Y., and H. Steller. 2015. Live to die another way: modes of programmed cell death and the signals emanating from dying cells. *Nat. Rev. Mol. Cell Biol.* 16:329–344. https://doi.org/10.1038/nrm3999

Gautheron, J., M. Vucur, F. Reisinger, D.V. Cardenas, C. Roderburg, C. Koppe, K. Kreggenwinkel, A.T. Schneider, M. Bartneck, U.P. Neumann, et al. 2014. A positive feedback loop between RIP3 and JNK controls non-alcoholic steatohepatitis. *EMBO Mol. Med.* 6:1062–1074. https://doi.org/10.15252/emmm.201403856

Geisler, S., R.A. Doan, A. Strickland, X. Huang, J. Milbrandt, and A. DiAntonio. 2016. Prevention of vincristine-induced peripheral neuropathy by genetic deletion of SARM1 in mice. *Brain.* 139:3092–3108. https://doi.org/10.1093/brain/aww251

Geisler, S., R.A. Doan, G.C. Cheng, A. Cetinkaya-Fisgin, S.X. Huang, A. Höke, J. Milbrandt, and A. DiAntonio. 2019a. Vincristine and bortezomib use distinct upstream mechanisms to activate a common SARM1-dependent axon degeneration program. *JCI Insight.* 4:e129920. https://doi.org/10.1172/jci.insight.129920

Geisler, S., S.X. Huang, A. Strickland, R.A. Doan, D.W. Summers, X. Mao, J. Park, A. DiAntonio, and J. Milbrandt. 2019b. Gene therapy targeting SARM1 blocks pathological axon degeneration in mice. *J. Exp. Med.* 216: 294–303. https://doi.org/10.1084/jem.20181040

Gerdts, J., D.W. Summers, Y. Sasaki, A. DiAntonio, and J. Milbrandt. 2013. Sarm1-mediated axon degeneration requires both SAM and TIR

interactions. *J. Neurosci.* 33:13569–13580. https://doi.org/10.1523/JNEUROSCI.1197-13.2013

Gerdts, J., E.J. Brace, Y. Sasaki, A. DiAntonio, and J. Milbrandt. 2015. SARM1 activation triggers axon degeneration locally via NAD+ destruction. *Science*. 348:453–457. https://doi.org/10.1126/science.1258366

Gerdts, J., D.W. Summers, J. Milbrandt, and A. DiAntonio. 2016. Axon Self-Destruction: New Links among SARM1, MAPKs, and NAD+ Metabolism. *Neuron*. 89:449–460. https://doi.org/10.1016/j.neuron.2015.12.023

Ghosh, A.S., B. Wang, C.D. Pozniak, M. Chen, R.J. Watts, and J.W. Lewcock. 2011. DLK induces developmental neuronal degeneration via selective regulation of proapoptotic JNK activity. *J. Cell Biol.* 194:751–764. https://doi.org/10.1083/jcb.201103153

Gilley, J., G. Orsomando, I. Nascimento-Ferreira, and M.P. Coleman. 2015. Absence of SARM1 rescues development and survival of NMNAT2-deficient axons. *Cell Rep.* 10:1974–1981. https://doi.org/10.1016/j.celrep.2015.02.060

Gong, Y.N., C. Guy, H. Olauson, J.U. Becker, M. Yang, P. Fitzgerald, A. Linkermann, and D.R. Green. 2017. ESCRT-III Acts Downstream of MLKL to Regulate Necroptotic Cell Death and Its Consequences. *Cell.* 169:286–300.e16. https://doi.org/10.1016/j.cell.2017.03.020

Hammond, T.R., S.E. Marsh, and B. Stevens. 2019. Immune Signaling in Neurodegeneration. *Immunity*. 50:955–974. https://doi.org/10.1016/j.immuni.2019.03.016

Hankins, H.M., R.D. Baldridge, P. Xu, and T.R. Graham. 2015. Role of flippases, scramblases and transfer proteins in phosphatidylserine subcellular distribution. *Traffic*. 16:35–47. https://doi.org/10.1111/tra.12233

Heckmann, B.L., B. Tummers, and D.R. Green. 2019. Crashing the computer: apoptosis vs. necroptosis in neuroinflammation. *Cell Death Differ.* 26:41–52. https://doi.org/10.1038/s41418-018-0195-3

Henninger, N., J. Bouley, E.M. Sikoglu, J. An, C.M. Moore, J.A. King, R. Bowser, M.R. Freeman, and R.H. Brown, Jr.. 2016. Attenuated traumatic axonal injury and improved functional outcome after traumatic brain injury in mice lacking *Sarm1*. *Brain*. 139:1094–1105. https://doi.org/10.1093/brain/aww001

Hernández, D.E., N.A. Salvadores, G. Moya-Alvarado, R.J. Catalán, F.C. Bronfman, and F.A. Court. 2018. Axonal degeneration induced by glutamate excitotoxicity is mediated by necroptosis. *J. Cell Sci.* 131. jcs214684. https://doi.org/10.1242/jcs.214684

Hickman, S., S. Izzy, P. Sen, L. Morsett, and J. El Khoury. 2018. Microglia in neurodegeneration. *Nat. Neurosci.* 21:1359–1369. https://doi.org/10.1038/s41593-018-0242-x

Howell, G.R., R.T. Libby, T.C. Jakobs, R.S. Smith, F.C. Phalan, J.W. Barter, J.M. Barbay, J.K. Marchant, N. Mahesh, V. Porciatti, et al. 2007. Axons of retinal ganglion cells are insulted in the optic nerve early in DBA/2J glaucoma. *J. Cell Biol.* 179:1523–1537. https://doi.org/10.1083/jcb.200706181

Huang, P., Y. Qi, Y.-S. Xu, J. Liu, D. Liao, S.S.-M. Zhang, and C. Zhang. 2010. Serum cytokine alteration is associated with optic neuropathy in human primary open angle glaucoma. *J. Glaucoma*. 19:324–330. https://doi.org/10.1097/IJG.0b013e3181b4cac7

Inman, D.M., and M. Harun-Or-Rashid. 2017. Metabolic Vulnerability in the Neurodegenerative Disease Glaucoma. *Front. Neurosci.* 11:146. https://doi.org/10.3389/fnins.2017.00146

Ito, Y., D. Ofengeim, A. Najafov, S. Das, S. Saberi, Y. Li, J. Hitomi, H. Zhu, H. Chen, L. Mayo, et al. 2016. RIPK1 mediates axonal degeneration by promoting inflammation and necroptosis in ALS. *Science*. 353:603–608. https://doi.org/10.1126/science.aaf6803

Kearney, C.J., and S.J. Martin. 2017. An Inflammatory Perspective on Necroptosis. *Mol. Cell.* 65:965–973. https://doi.org/10.1016/j.molcel.2017.02.024

Kerrigan-Baumrind, L.A., H.A. Quigley, M.E. Pease, D.F. Kerrigan, and R.S. Mitchell. 2000. The number of retinal ganglion cells in glaucoma eyes compared to threshold visual field data in the same eyes. *Invest. Ophthalmol. Vis. Sci.* 41:741–748.

Kitaoka, Y., Y. Kitaoka, J.M. Kwong, F.N. Ross-Cisneros, J. Wang, R.K. Tsai, A.A. Sadun, and T.T. Lam. 2006. TNF-α-induced optic nerve degeneration and nuclear factor-kappaB p65. *Invest. Ophthalmol. Vis. Sci.* 47:1448–1457. https://doi.org/10.1167/iovs.05-0299

Kitaoka, Y., Y. Hayashi, T. Kumai, H. Takeda, Y. Munemasa, H. Fujino, Y. Kitaoka, S. Ueno, A.A. Sadun, and T.T. Lam. 2009. Axonal and cell body protection by nicotinamide adenine dinucleotide in tumor necrosis factor-induced optic neuropathy. *J. Neuropathol. Exp. Neurol.* 68:915–927. https://doi.org/10.1097/NEN.0b013e3181afecfa

Kitaoka, Y., Y. Munemasa, K. Kojima, A. Hirano, S. Ueno, and H. Takagi. 2013. Axonal protection by Nmnat3 overexpression with involvement of autophagy in optic nerve degeneration. *Cell Death Dis.* 4. e860. https://doi.org/10.1038/cddis.2013.391

Leon, S., Y. Yin, J. Nguyen, N. Irwin, and L.I. Benowitz. 2000. Lens injury stimulates axon regeneration in the mature rat optic nerve. *J. Neurosci.* 20:4615–4626. https://doi.org/10.1523/JNEUROSCI.20-12-04615.2000

Libby, R.T., Y. Li, O.V. Savinova, J. Barter, R.S. Smith, R.W. Nickells, and S.W.M. John. 2005. Susceptibility to neurodegeneration in a glaucoma is modified by Bax gene dosage. *PLoS Genet.* 1:17–26. https://doi.org/10.1371/journal.pgen.0010004

Loreto, A., C.S. Hill, V.L. Hewitt, G. Orsomando, C. Angeletti, J. Gilley, C. Lucci, A. Sanchez-Martinez, A.J. Whitworth, L. Conforti, et al. 2020. Mitochondrial impairment activates the Wallerian pathway through depletion of NMNAT2 leading to SARM1-dependent axon degeneration. *Neurobiol. Dis.* 134. 104678. https://doi.org/10.1016/j.nbd.2019.104678

Maino, B., S. Paparone, C. Severini, M.T. Ciotti, V. D'agata, P. Calissano, and S. Cavallaro. 2017. Drug target identification at the crossroad of neuronal apoptosis and survival. *Expert Opin. Drug Discov.* 12:249–259. https://doi.org/10.1080/17460441.2017.1280023

Mattson, M.P.. 2000. Apoptosis in neurodegenerative disorders. *Nat. Rev. Mol. Cell Biol.* 1:120–129. https://doi.org/10.1038/35040009

McNamara, C.R., R. Ahuja, A.D. Osafo-Addo, D. Barrows, A. Kettenbach, I. Skidan, X. Teng, G.D. Cuny, S. Gerber, and A. Degterev. 2013. Akt Regulates TNFα synthesis downstream of RIP1 kinase activation during necroptosis. *PLoS One*. 8. e56576. https://doi.org/10.1371/journal.pone.0056576

Mukherjee, P., T.A. Woods, R.A. Moore, and K.E. Peterson. 2013. Activation of the innate signaling molecule MAVS by bunyavirus infection upregulates the adaptor protein SARM1, leading to neuronal death. *Immunity*. 38:705–716. https://doi.org/10.1016/j.immuni.2013.02.013

Nakazawa, T., C. Nakazawa, A. Matsubara, K. Noda, T. Hisatomi, H. She, N. Michaud, A. Hafezi-Moghadam, J.W. Miller, and L.I. Benowitz. 2006. Tumor necrosis factor-alpha mediates oligodendrocyte death and delayed retinal ganglion cell loss in a mouse model of glaucoma. *J. Neurosci.* 26:12633–12641. https://doi.org/10.1523/JNEUROSCI.2801-06.2006

Ofengeim, D., Y. Ito, A. Najafov, Y. Zhang, B. Shan, J.P. DeWitt, J. Ye, X. Zhang, A. Chang, H. Vakifahmetoglu-Norberg, et al. 2015. Activation of necroptosis in multiple sclerosis. *Cell Rep.* 10:1836–1849. https://doi.org/10.1016/j.celrep.2015.02.051

Oñate, M., A. Catenaccio, N. Salvadores, C. Saquel, A. Martinez, I. Moreno-Gonzalez, N. Gamez, P. Soto, C. Soto, C. Hetz, and F.A. Court. 2020. The necroptosis machinery mediates axonal degeneration in a model of Parkinson disease. *Cell Death Differ.* 27:1169–1185.

Orozco, S., N. Yatim, M.R. Werner, H. Tran, S.Y. Gunja, S.W.G. Tait, M.L. Albert, D.R. Green, and A. Oberst. 2014. RIPK1 both positively and negatively regulates RIPK3 oligomerization and necroptosis. *Cell Death Differ.* 21:1511–1521. https://doi.org/10.1038/cdd.2014.76

Payne, S.C., C.A. Bartlett, D.L. Savigni, A.R. Harvey, S.A. Dunlop, and M. Fitzgerald. 2013. Early proliferation does not prevent the loss of oligodendrocyte progenitor cells during the chronic phase of secondary degeneration in a CNS white matter tract. *PLoS One*. 8. e65710. https://doi.org/10.1371/journal.pone.0065710

Perry, V.H., and C. Holmes. 2014. Microglial priming in neurodegenerative disease. *Nat. Rev. Neurol.* 10:217–224. https://doi.org/10.1038/nrneurol.2014.38

Remtulla, S., and P.E. Hallett. 1985. A schematic eye for the mouse, and comparisons with the rat. *Vision Res.* 25:21–31. https://doi.org/10.1016/0042-6989(85)90076-8

Roh, M., Y. Zhang, Y. Murakami, A. Thanos, S.C. Lee, D.G. Vavvas, L.I. Benowitz, and J.W. Miller. 2012. Etanercept, a widely used inhibitor of tumor necrosis factor-α (TNF-α), prevents retinal ganglion cell loss in a rat model of glaucoma. *PLoS One*. 7. e40065. https://doi.org/10.1371/journal.pone.0040065

Sasaki, Y., T. Nakagawa, X. Mao, A. DiAntonio, and J. Milbrandt. 2016. NMNAT1 inhibits axon degeneration via blockade of SARM1-mediated NAD+ depletion. *eLife*. 5. e19749. https://doi.org/10.7554/eLife.19749

Sasaki, Y., T.M. Engber, R.O. Hughes, M.D. Figley, T. Wu, T. Bosanac, R. Devraj, J. Milbrandt, R. Krauss, and A. DiAntonio. 2020. cADPR is a gene dosage-sensitive biomarker of SARM1 activity in healthy, compromised, and degenerating axons. *Exp. Neurol.* 329. 113252. https://doi.org/10.1016/j.expneurol.2020.113252

Sawada, H., T. Fukuchi, T. Tanaka, and H. Abe. 2010. Tumor necrosis factor-α concentrations in the aqueous humor of patients with glaucoma. *Invest. Ophthalmol. Vis. Sci.* 51:903–906. https://doi.org/10.1167/iovs.09-4247

Seitz, R., and E.R. Tamm. 2014. Müller Cells and Microglia of the Mouse Eye React Throughout the Entire Retina in Response to the Procedure of an

Intravitreal Injection. Springer, New York, NY. pp. 347–353. https://doi.org/10.1007/978-1-4614-3209-8_44

Sharma, S., S.L. Ball, and N.S. Peachey. 2005. Pharmacological studies of the mouse cone electroretinogram. *Vis. Neurosci.* 22:631–636. https://doi.org/10.1017/S0952523805225129

Shin, J.E., B.R. Miller, E. Babetto, Y. Cho, Y. Sasaki, S. Qayum, E.V. Russler, V. Cavalli, J. Milbrandt, and A. DiAntonio. 2012. SCG10 is a JNK target in the axonal degeneration pathway. *Proc. Natl. Acad. Sci. USA.* 109: E3696–E3705. https://doi.org/10.1073/pnas.1216204109

Silke, J., J.A. Rickard, and M. Gerlic. 2015. The diverse role of RIP kinases in necroptosis and inflammation. *Nat. Immunol.* 16:689–697. https://doi.org/10.1038/ni.3206

Simon, D.J., and T.A. Watkins. 2018. Therapeutic opportunities and pitfalls in the treatment of axon degeneration. *Curr. Opin. Neurol.* 31:693–701. https://doi.org/10.1097/WCO.0000000000000621

Son, J.L., I. Soto, E. Oglesby, T. Lopez-Roca, M.E. Pease, H.A. Quigley, and N. Marsh-Armstrong. 2010. Glaucomatous optic nerve injury involves early astrocyte reactivity and late oligodendrocyte loss. *Glia.* 58: 780–789. https://doi.org/10.1002/glia.20962

Su, L., B. Quade, H. Wang, L. Sun, X. Wang, and J. Rizo. 2014. A plug release mechanism for membrane permeation by MLKL. *Structure.* 22: 1489–1500. https://doi.org/10.1016/j.str.2014.07.014

Summers, D.W., A. DiAntonio, and J. Milbrandt. 2014. Mitochondrial dysfunction induces Sarm1-dependent cell death in sensory neurons. *J. Neurosci.* 34:9338–9350. https://doi.org/10.1523/JNEUROSCI.0877-14.2014

Summers, D.W., J. Milbrandt, and A. DiAntonio. 2018. Palmitoylation enables MAPK-dependent proteostasis of axon survival factors. *Proc. Natl. Acad. Sci. USA.* 115:E8746–E8754. https://doi.org/10.1073/pnas.1806933115

Summers, D.W., E. Frey, L.J. Walker, J. Milbrandt, and A. DiAntonio. 2020. DLK Activation Synergizes with Mitochondrial Dysfunction to Downregulate Axon Survival Factors and Promote SARM1-Dependent Axon Degeneration. *Mol. Neurobiol.* 57:1146–1158. https://doi.org/10.1007/s12035-019-01796-2

Syc-Mazurek, S.B., and R.T. Libby. 2019. Axon injury signaling and compartmentalized injury response in glaucoma. *Prog. Retin. Eye Res.* 73. 100769. https://doi.org/10.1016/j.preteyeres.2019.07.002

Szretter, K.J., M.A. Samuel, S. Gilfillan, A. Fuchs, M. Colonna, and M.S. Diamond. 2009. The immune adaptor molecule SARM modulates tumor necrosis factor alpha production and microglia activation in the brainstem and restricts West Nile Virus pathogenesis. *J. Virol.* 83: 9329–9338. https://doi.org/10.1128/JVI.00836-09

Tanzer, M.C., I. Matti, J.M. Hildebrand, S.N. Young, A. Wardak, A. Tripaydonis, E.J. Petrie, A.L. Mildenhall, D.L. Vaux, J.E. Vince, et al. 2016. Evolutionary divergence of the necroptosis effector MLKL. *Cell Death Differ.* 23:1185–1197. https://doi.org/10.1038/cdd.2015.169

Tezel, G., and M.B. Wax. 2004. The immune system and glaucoma. *Curr. Opin. Ophthalmol.* 15:80–84. https://doi.org/10.1097/00055735-200404000-00003

Tezel, G., L.Y. Li, R.V. Patil, and M.B. Wax. 2001. TNF-α and TNF-α receptor-1 in the retina of normal and glaucomatous eyes. *Invest. Ophthalmol. Vis. Sci.* 42:1787–1794.

Vitner, E.B., R. Salomon, T. Farfel-Becker, A. Meshcheriakova, M. Ali, A.D. Klein, F.M. Platt, T.M. Cox, and A.H. Futerman. 2014. RIPK3 as a potential therapeutic target for Gaucher's disease. *Nat. Med.* 20:204–208. https://doi.org/10.1038/nm.3449

Walker, L.J., D.W. Summers, Y. Sasaki, E.J. Brace, J. Milbrandt, and A. DiAntonio. 2017. MAPK signaling promotes axonal degeneration by speeding the turnover of the axonal maintenance factor NMNAT2. *eLife.* 6. e22540. https://doi.org/10.7554/eLife.22540

Wang, Z., H. Jiang, S. Chen, F. Du, and X. Wang. 2012. The mitochondrial phosphatase PGAM5 functions at the convergence point of multiple necrotic death pathways. *Cell.* 148:228–243. https://doi.org/10.1016/j.cell.2011.11.030

Wang, H., L. Sun, L. Su, J. Rizo, L. Liu, L.F. Wang, F.S. Wang, and X. Wang. 2014. Mixed lineage kinase domain-like protein MLKL causes necrotic membrane disruption upon phosphorylation by RIP3. *Mol. Cell.* 54: 133–146. https://doi.org/10.1016/j.molcel.2014.03.003

Weinlich, R., A. Oberst, H.M. Beere, and D.R. Green. 2017. Necroptosis in development, inflammation and disease. *Nat. Rev. Mol. Cell Biol.* 18: 127–136. https://doi.org/10.1038/nrm.2016.149

Weinreb, R.N., T. Aung, and F.A. Medeiros. 2014. The pathophysiology and treatment of glaucoma: a review. *JAMA.* 311:1901–1911. https://doi.org/10.1001/jama.2014.3192

Welsbie, D.S., Z. Yang, Y. Ge, K.L. Mitchell, X. Zhou, S.E. Martin, C.A. Berlinicke, L. Hackler, Jr., J. Fuller, J. Fu, et al. 2013. Functional genomic screening identifies dual leucine zipper kinase as a key mediator of retinal ganglion cell death. *Proc. Natl. Acad. Sci. USA.* 110:4045–4050. https://doi.org/10.1073/pnas.1211284110

Williams, P.A., J.M. Harder, N.E. Foxworth, B.H. Cardozo, K.E. Cochran, and S.W.M. John. 2017a. Nicotinamide and WLD^S Act Together to Prevent Neurodegeneration in Glaucoma. *Front. Neurosci.* 11:232. https://doi.org/10.3389/fnins.2017.00232

Williams, P.A., J.M. Harder, N.E. Foxworth, K.E. Cochran, V.M. Philip, V. Porciatti, O. Smithies, and S.W.M. John. 2017b. Vitamin B_3 modulates mitochondrial vulnerability and prevents glaucoma in aged mice. *Science.* 355:756–760. https://doi.org/10.1126/science.aal0092

Williams, P.A., N. Marsh-Armstrong, G.R. Howell, A. Bosco, J. Danias, J. Simon, A. Di Polo, M.H. Kuehn, S. Przedborski, M. Raff, et al. Lasker/IRRF Initiative on Astrocytes and Glaucomatous Neurodegeneration Participants. 2017c. Neuroinflammation in glaucoma: A new opportunity. *Exp. Eye Res.* 157:20–27. https://doi.org/10.1016/j.exer.2017.02.014

Xia, B., S. Fang, X. Chen, H. Hu, P. Chen, H. Wang, and Z. Gao. 2016. MLKL forms cation channels. *Cell Res.* 26:517–528. https://doi.org/10.1038/cr.2016.26

Yan, X., G. Tezel, M.B. Wax, and D.P. Edward. 2000. Matrix metalloproteinases and tumor necrosis factor α in glaucomatous optic nerve head. *Arch. Ophthalmol.* 118:666–673. https://doi.org/10.1001/archopht.118.5.666

Yang, J., Z. Wu, N. Renier, D.J. Simon, K. Uryu, D.S. Park, P.A. Greer, C. Tournier, R.J. Davis, and M. Tessier-Lavigne. 2015. Pathological axonal death through a MAPK cascade that triggers a local energy deficit. *Cell.* 160:161–176. https://doi.org/10.1016/j.cell.2014.11.053

Yin, L., K. Greenberg, J.J. Hunter, D. Dalkara, K.D. Kolstad, B.D. Masella, R. Wolfe, M. Visel, D. Stone, R.T. Libby, et al. 2011. Intravitreal injection of AAV2 transduces macaque inner retina. *Invest. Ophthalmol. Vis. Sci.* 52: 2775–2783. https://doi.org/10.1167/iovs.10-6250

Yu, D.-Y., and S.J. Cringle. 2006. Oxygen distribution in the mouse retina. *Invest. Ophthalmol. Vis. Sci.* 47:1109–1112. https://doi.org/10.1167/iovs.05-1118

Yuan, J., P. Amin, and D. Ofengeim. 2019. Necroptosis and RIPK1-mediated neuroinflammation in CNS diseases. *Nat. Rev. Neurosci.* 20:19–33. https://doi.org/10.1038/s41583-018-0093-1

Zhang, J., Y. Yang, W. He, and L. Sun. 2016. Necrosome core machinery: MLKL. *Cell. Mol. Life Sci.* 73:2153–2163. https://doi.org/10.1007/s00018-016-2190-5

Zhang, S., M.B. Tang, H.Y. Luo, C.H. Shi, and Y.M. Xu. 2017. Necroptosis in neurodegenerative diseases: a potential therapeutic target. *Cell Death Dis.* 8. e2905. https://doi.org/10.1038/cddis.2017.286

Zhu, Y., L. Zhang, Y. Sasaki, J. Milbrandt, and J.M. Gidday. 2013. Protection of mouse retinal ganglion cell axons and soma from glaucomatous and ischemic injury by cytoplasmic overexpression of Nmnat1. *Invest. Ophthalmol. Vis. Sci.* 54:25–36. https://doi.org/10.1167/iovs.12-10861

Supplemental material

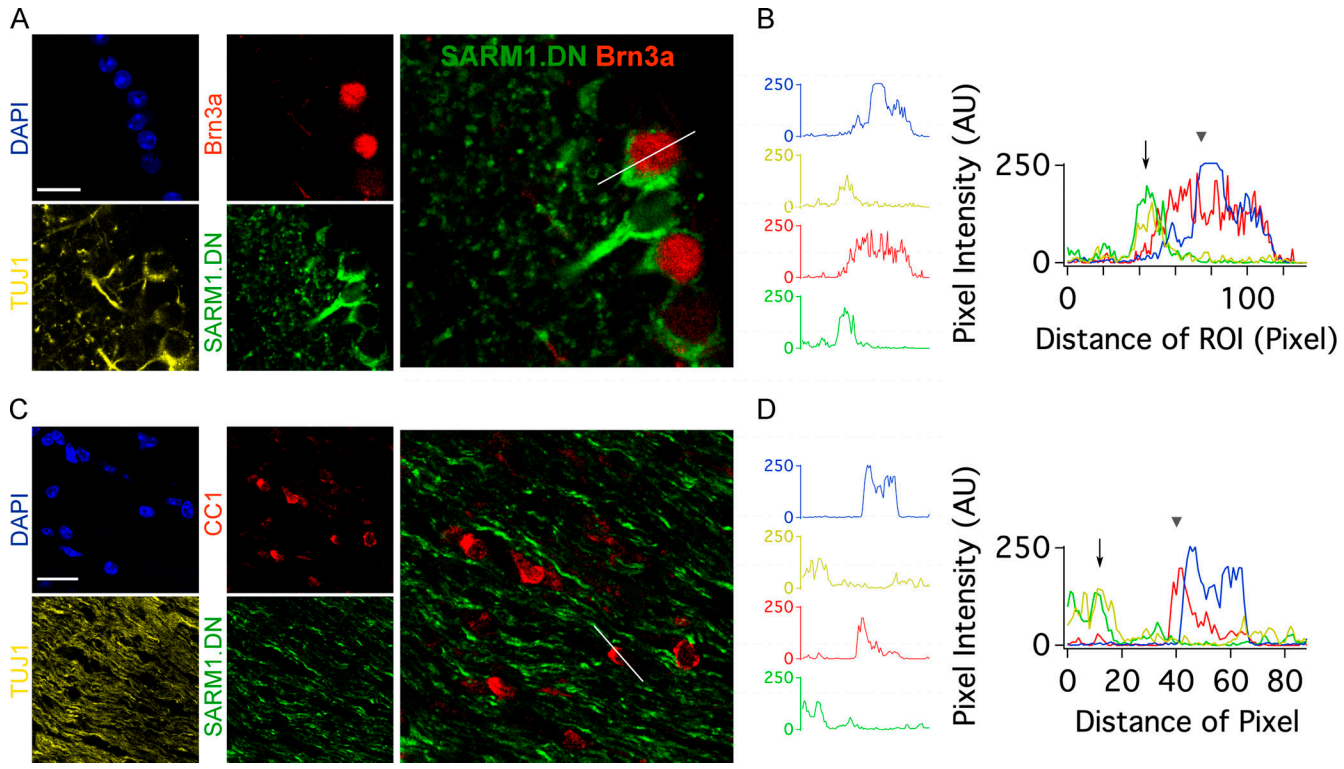

Figure S1. **Intravitreal injection of AAV-hSyn-SARM1.DN-EGFP drives expression in RGCs but not oligodendrocytes. (A)** Representative confocal single section images of retina (cross-section) following intravitreal injection of AAV-hSyn-SARM1.DN.EGFP. Retina are stained for nuclei (DAPI, blue), axons (TUJ1, yellow), RGC nuclei (Brn3a, red), and SARM1.DN (green). The white line is the region of interest for the analysis of pixel intensity of each channel. Scale bar, 20 µm. **(B)** Pixel intensity analysis for the region of interest from A. The RGC nuclear marker Brn3a overlaps with DAPI staining (arrowhead) while the adjacent GFP signal of SARM1.DN overlaps with TUJ1 (arrow). SARM1.DN is detected in the cytosol of RGCs. **(C)** Representative confocal single section images of optic nerve (longitudinal section) following intravitreal injection of AAV-hSyn-SARM1.DN.EGFP. Optic nerve is stained for nuclei (DAPI, blue), axons (TUJ1, yellow), oligodendrocyte nuclei (CC1, red), and SARM1.DN (green). The white line is the region of interest for the analysis of pixel intensity of each channel. Scale bar, 20 µm. **(D)** Pixel intensity analysis for the region of interest from A. The mature oligodendrocyte nuclear marker CC1 overlaps with DAPI staining (arrowhead) but is distant from the axonal staining of SARM1.DN and TUJ1 (arrow) consistent with RGC expression of SARM1.DN. AU, arbitray units; ROI, region of interest.

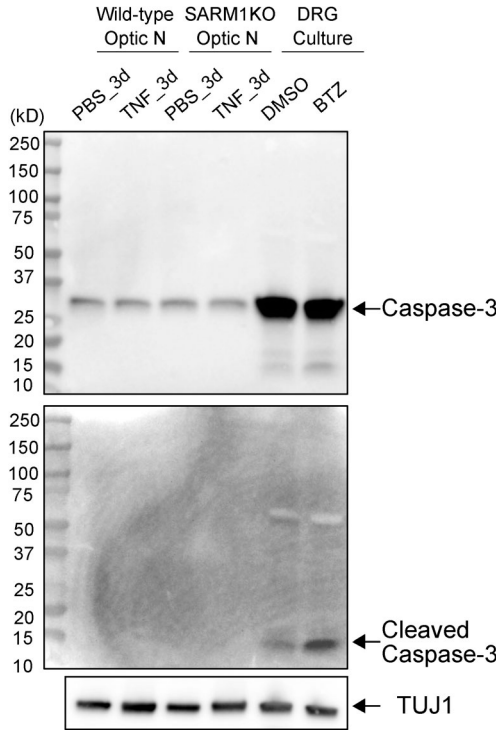

Figure S2. **Cleaved caspase 3 is not detected in optic nerve of TNF-α injected eyes.** Immunoblot of optic nerve (Optic N) extracts stained for caspase-3 (top), cleaved caspase-3 (middle), and TUJ1 (bottom) as a loading control. Samples are collected from optic nerves 3 d after TNF-α or PBS injection (lanes 1–4). These samples were also used for Fig. 2, I and J. Because cleaved caspse-3 is not detected in TNF-α–injected optic nerves, cultured DRG neurons were incubated with either DMSO (lane 5) or 100 nM bortezomib (BTZ, lane 6) for 18 h as a positive control (Geisler et al., 2019a).

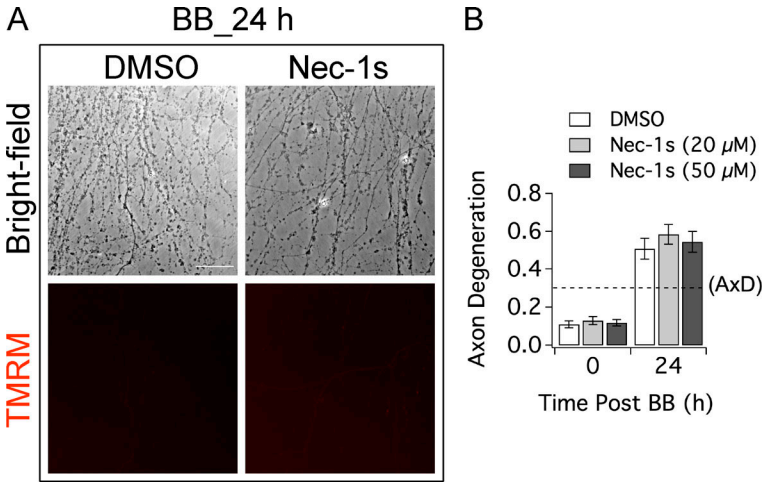

Figure S3. **Necrostatin-1s does not prevent axon degeneration following dimerization of MLKL.ND. (A)** Representative bright-field and TMRM images for DRG neurons expressing MLKL.ND 24 h after BB addition. The neurons were treated with either DMSO (control) or necrostatin-1s (Nec-1s) 30 min before BB addition. Scale bar, 50 µm. **(B)** Quantitative analysis of axon degeneration at 0 h and 24 h after BB application from bright-field images for neurons treated with DMSO or the indicated dose of necrostatin-1s. Necrostatin-1s does not block axon degeneration, consistent with MLKL.ND functioning after RIPK1 in the necroptosis pathway. Axons with a DI >0.3 are defined as degenerated (dashed line). Data represent the mean ± SEM, n = 5; two-way ANOVA with post hoc Bonferroni's multiple comparison test; time, $F(1, 9) = 257.4$, $P < 0.0001$; interaction, $F(9, 9) = 2.513$, $P = 0.0930$; *, $P < 0.05$; **, $P < 0.01$; and ***, $P < 0.001$.

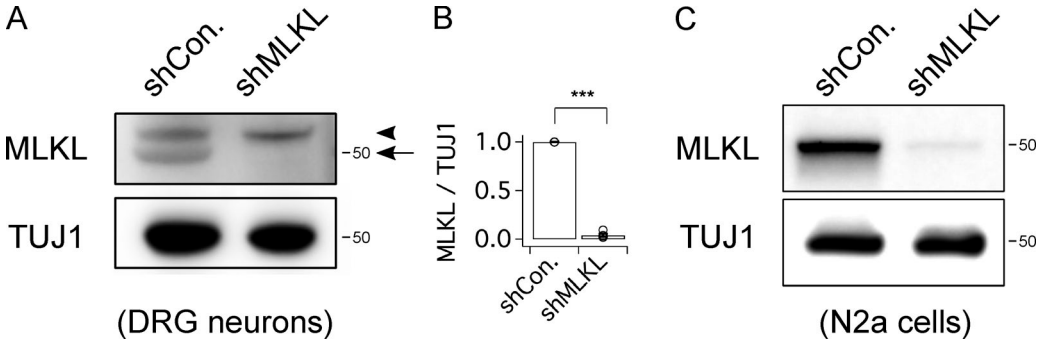

Figure S4. **Validation of shRNA for MLKL in cultured DRG neurons and N2a cells. (A)** Immunoblot analysis of MLKL from DRG neurons expressing control shRNA (shCon) or MLKL targeted shRNA. Arrow (MLKL band), arrowhead (nonspecific band). TUJ1 is used as a loading control. **(B)** Quantification of MLKL knockdown in DRG neurons expressing shMLKL as in A. Data represent the mean ± SEM, $n = 5$; two-tailed unpaired t test, $P < 0.0001$; *, $P < 0.05$; **, $P < 0.01$; and ***, $P < 0.001$. **(C)** Immunoblot analysis of MLKL from N2a cells expressing control or MLKL targeted shRNA. TUJ1 is used as a loading control.

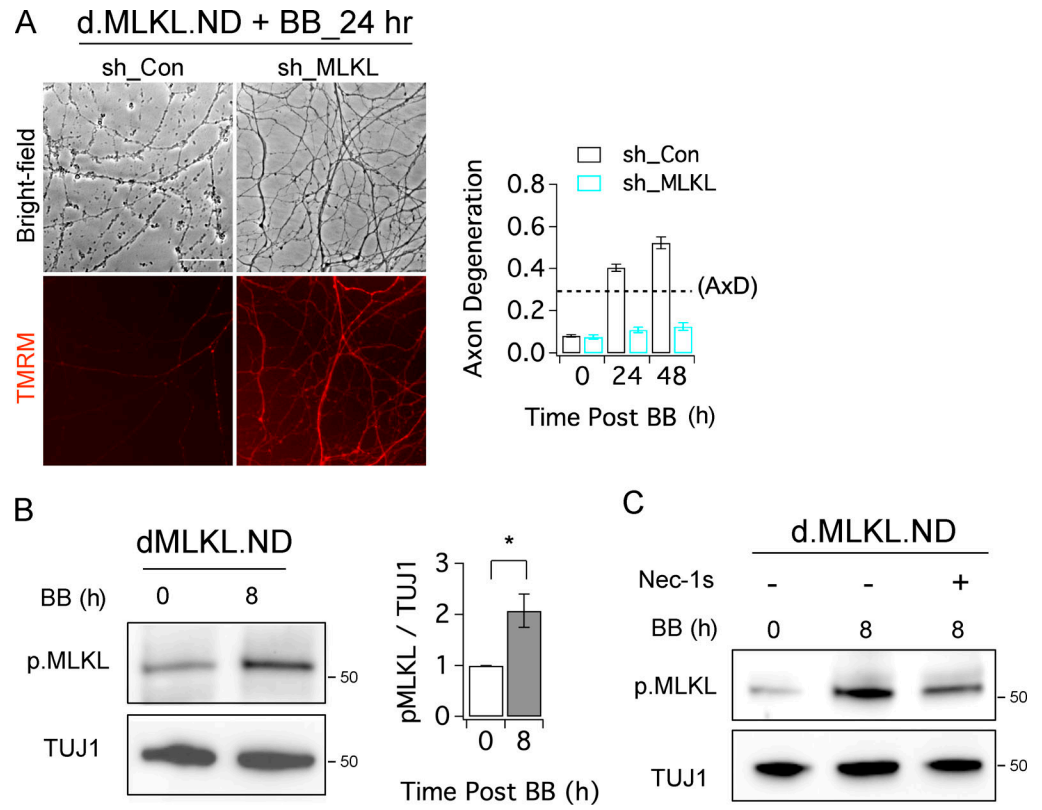

Figure S5. **Dimerized MLKL.ND requires endogenous MLKL to induce axon degeneration. (A)** Left: Representative bright-field and TMRM images of axons from DRG neurons expressing MLKL.ND 24 h after BB addition. Neurons express either control or MLKL targeted shRNA. The MLKL shRNA targets the C-terminal half of MLKL and therefore does not recognize MLKL.ND. Scale bar, 50 µm. Right: Quantitative analysis of axon degeneration at the indicated times after BB application for the indicted conditions. Axons expressing shRNA to endogenous MLKL are protected for at least 48 h after dimerization of MLKL.ND. Axons with a DI >0.3 are defined as degenerated (dashed line). Data represent the mean ± SEM, $n = 4$; two-way ANOVA with post hoc Bonferroni's multiple comparison test; time, $F(1.116, 6.695) = 159.4$; *, $P < 0.05$; **, $P < 0.01$; and ***, $P < 0.001$. **(B)** Left: Immunoblot of phosphorylated MLKL in lysates from neurons expressing MLKL.ND collected at 0 or 8 h after BB addition. TUJ1 is used as a loading control. Dimerization of MLKL.ND triggers phosphorylation of endogenous MLKL. Right: Quantification of phosphorylated MLKL levels normalized to TUJ1. Data represent the mean ± SEM, $n = 3$; two-tailed unpaired t test, $P = 0.0283$; *, $P < 0.05$; **, $P < 0.01$; and ***, $P < 0.001$. **(C)** Immunoblot analysis as in B but including necrostatin-1s addition where indicated. This experiment demonstrates that treatment with the RIPK1 inhibitor necrostatin-1s does not prevent the phosphorylation of MLKL induced by dimerization of MLKL.ND. These data in conjunction with Fig. S3 demonstrate that MLKL.ND does not require upstream RIPK1.

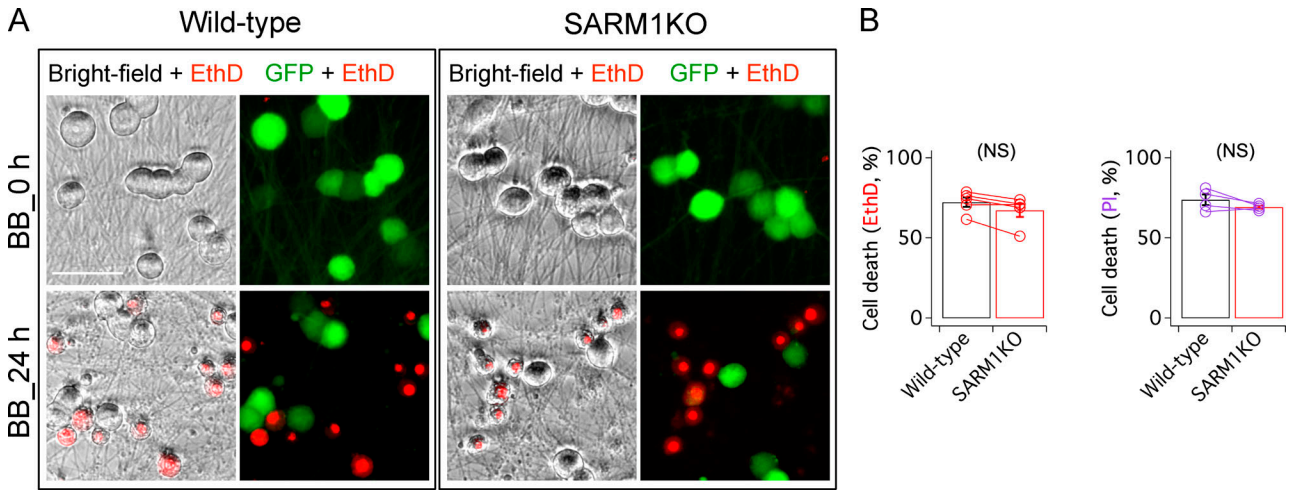

Figure S6. **SARM1 KO does not prevent cell death induced by dimerization of MLKL.ND. (A)** Representative bright-field and fluorescent images at 0 or 24 h after BB addition to WT or SARM1 KO DRG neurons that both express MLKL.ND and cytosolic GFP. Cells are stained with EthD (red) and imaged for GFP (green) to identify dead cells ($EthD^+$ and GFP^-). Scale bar, 50 µm. **(B)** Quantification of cell death of WT and SARM1 KO DRG neurons expressing MLKL.ND with two different markers for cell death 24 h after BB application. Left: EthD, $n = 5$; PI, $n = 4$; Data represent the mean ± SEM; for EthD, two-tailed unpaired t test, $P = 0.34$; for PI, two-tailed unpaired t test, $P = 0.23$.

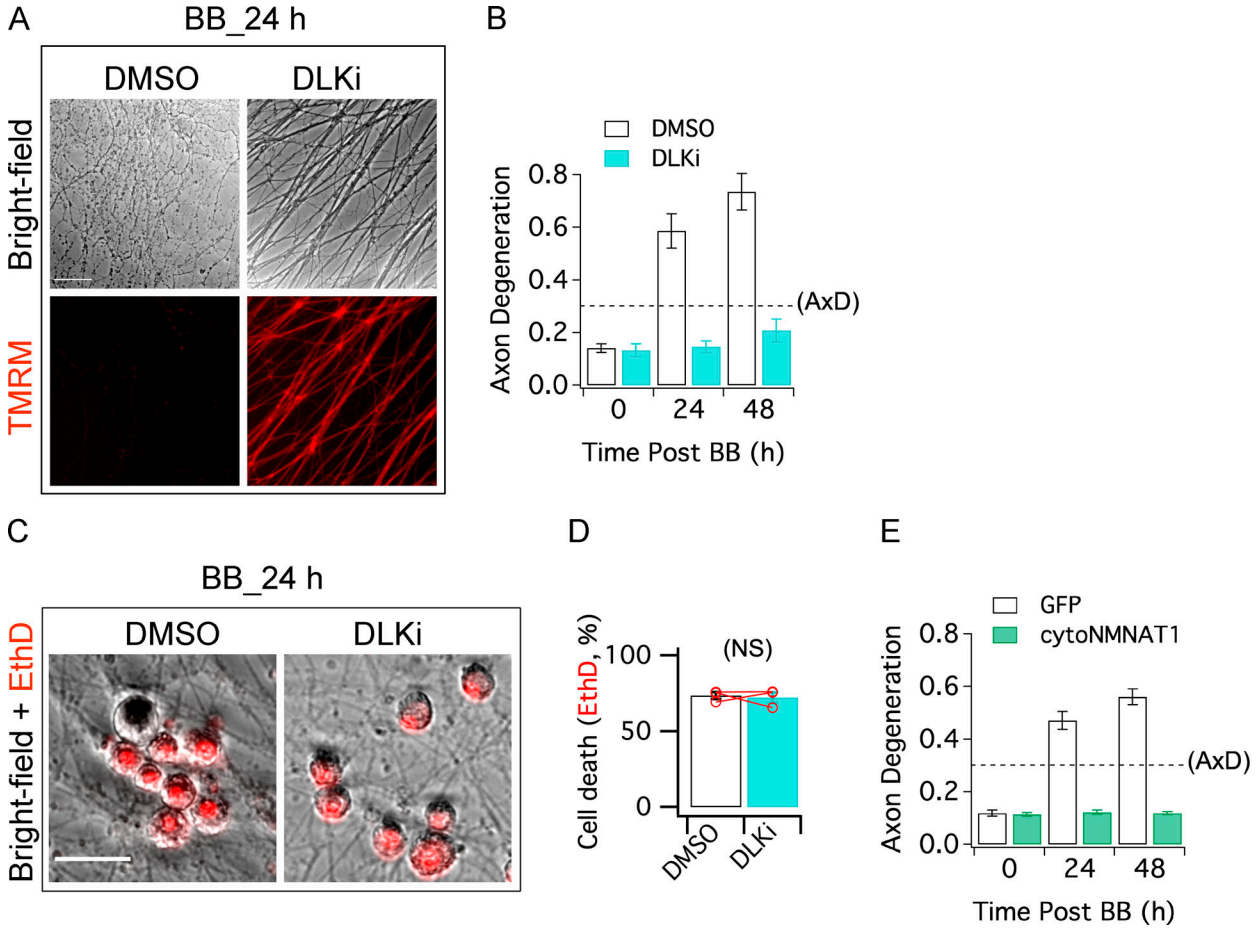

Figure S7. **DLK inhibition and cytoNMNAT1 expression block axon degeneration induced by dimerization of MLKL.ND. (A)** Representative bright-field and TMRM images of axons from WT DRG neurons expressing MLKL.ND at 24 h after BB treatment. Neurons were pretreated with DMSO or 500 nM DLK inhibitor (DLKi; GNE-3511). Scale bar, 50 µm. **(B)** Quantification of axon degeneration at the indicated times after BB (100 nM) application for the conditions described in A. DLK inhibition blocks axon degeneration for at least 48 h after BB application. Axons with a DI >0.3 are defined as degenerated (dashed line). Data represent the mean ± SEM, $n = 4$; two-way ANOVA with post hoc Bonferroni's multiple comparison test; time, $F(1.910, 9.552) = 62.13$, $P < 0.0001$; *, $P < 0.05$; **, $P < 0.01$; and ***, $P < 0.001$. **(C)** Representative bright-field and EthD fluorescent images of neuronal cell bodies for the conditions described in A at 24 h after BB application. Scale bar, 30 µm. **(D)** Quantification of neuronal cell death ($EthD^+$) 24 h after BB treatment for the conditions described in A. DLK inhibitor does not block cell death. Data represent the mean ± SEM, $n = 3$; two-tailed unpaired t test, $P = 0.78$. **(E)** Quantification of axon degeneration in WT neurons expressing MLKL.ND and infected with lentivirus expressing EGFP (FUGW control) the axon survival factor cytoNMNAT1. Expression of cytoNMNAT1 blocks axon degeneration induced by MLKL.ND dimerization. Axons with a DI >0.3 are defined as degenerated (dashed line). Data represent the mean ± SEM, $n = 5$; two-way ANOVA with post hoc Bonferroni's multiple comparison test; time, $F(1.863, 14.90) = 144.8$, $P < 0.0001$; interaction, $F(8, 16) = 4.061$, $P = 0.0082$; *, $P < 0.05$; **, $P < 0.01$; and ***, $P < 0.001$.

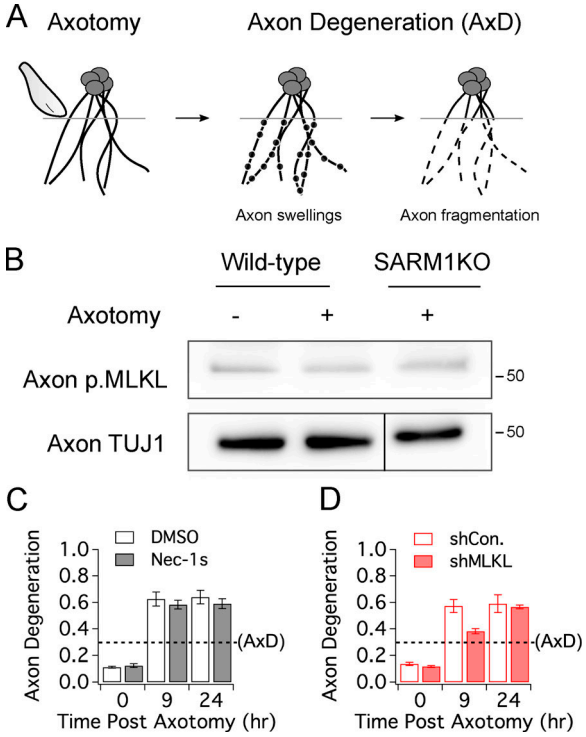

Figure S8. **Necroptosis is not activated by nor required for Wallerian degeneration. (A)** Schematic diagram of axotomy-induced Wallerian degeneration in cultured DRG neurons. **(B)** To assess whether axotomy activates the necroptotic pathway leading to the phosphorylation of MLKL, axon lysates are collected at 0 and 3 h after axotomy from WT DRG neurons and at 3 h after axotomy from SARM1 KO DRG neurons. 3 h after axotomy was chosen because this is the time point at which SARM1 is activated and severed axons are committed to degenerate. MLKL is not phosphorylated in response to axon transection. **(C)** To determine if necrostatin-1s blocks Wallerian degeneration, WT DRG neurons were treated with 20 µM necrostatin-1s (Nec-1s) 30 min before axon severing. Axon degeneration was quantified at 0, 9, and 24 h after axotomy. Axons with a DI >0.3 are defined as degenerated (dashed line). Note that necrostatin-1s does not block degeneration of severed axons. Data represent the mean ± SEM, n = 3; two-way ANOVA with post hoc Bonferroni's multiple comparison test; time, $F(1.008, 4.031) = 168.9$, $P = 0.0002$; interaction, $F(4, 8) = 2.284$, $P = 0.1488$; *, $P < 0.05$; **, $P < 0.01$; and ***, $P < 0.001$. **(D)** To determine if genetic loss of MLKL blocks Wallerian degeneration, WT DRG neurons were treated with a control or MLKL targeted shRNA as in S4 and S5. Axon degeneration was quantified at 0, 9, and 24 h after axotomy. Axons with a DI >0.3 are defined as degenerated (dashed line). Knockdown of MLKL does not block degeneration of severed axons. Data represent the mean ± SEM, n = 4; two-way ANOVA with post hoc Bonferroni's multiple comparison test; time, $F(1.142, 6.854) = 230.8$, $P < 0.0001$; interaction, $F(6, 12) = 5.801$, $P = 0.0048$; *, $P < 0.05$; **, $P < 0.01$; and ***, $P < 0.001$.

Video 1. **Calcium influx by dimerization of MLKL.ND is completely prevented in axons from SARM1 KO neurons.** Live-cell images of WT and SARM1 KO axons infected with lentivirus encoding GCaMP6 and mRuby3. After BB (100 nM) application, images were acquired every 1 h.

Video 2. **Local calcium influx in axons, not in soma by dimerization of MLKL.ND.** Live-cell images of WT and SARM1 KO neurons cultured in microfluidic devices. BB is only applied to the axon compartment. Images were acquired every 1 h.

Table S1 is provided online as a separate file and shows reagents used in the study.